The Effects of Minerals on Reservoir Properties in Block 3A and 2C, within the Orange Basin, South Africa.

Sadiya Salie

A thesis submitted in the fulfilment of the requirements for the degree of

Magister Scientiae

In

Applied Geology

Department of Earth Science, Faculty of Sciences, University of the Western Cape

Supervisor: Dr. M. Opuwari

Co-Supervisor: T. Chatterjee

April 2018

Declaration

I declare “The effects of minerals on Reservoir Properties in Block 3A and 2C, within the Orange basin, Offshore South Africa” is my own work, that it has not been submitted before for any degree or examination in any other university, and that all the sources I have used or quoted have been indicated and acknowledged by means of complete references.

Sadiya Salie April 2018

S.salie

Signature

Abstract

The reservoir quality of the Orange Basin, offshore South Africa is known to be immensely impaired by the presence of authigenic minerals. The collective effects of burial, bioturbation, compaction and chemical reactions between rocks, fluid and organic matter conclusively determined the quality of reservoirs within the Orange basin.

The aim of this study was to provide information on the quality of reservoirs within the Orange Basin. Data used to conduct this study include wireline logs (LAS format), well completion reports and core samples from potential reservoir zones of wells K-A2, K-A3 and K-E1. To accomplish the aim, petrophysical parameters were calculated, such as porosity, permeability and water saturation. Besides, depositional environments were identified using gamma ray log and core logging techniques. Thirdly, petrographic studies were supporting techniques in understanding how various minerals and diagenetic processes play a role in reservoir characterisation.

Geophysical wireline logs (Gamma ray, Resistivity, Bulk density and Caliper) allowed for the estimation of the three main reservoir properties; namely: porosity, water saturation and permeability.

The porosity calculations revealed a range of 3-18% for well K-A2, 2%-13% for well K-A3 and 3%-16% for well K-E1. The permeability's ranged from 0.08-0.1 mD and 0.001-1.30 mD for K-A3 and K-E1, respectively. Thus, the findings of the petrophysical evaluation of the wells in Interactive Petrophysics indicated that the reservoir intervals of wells K-A2, K-A3 and K-E1 are of poor to good quality. Based on the core analyses, the depositional environment is mostly shallow marine, specifically tide dominated for well K-A2, sandstone channel for well K-A3 and intertidal environment for well K-E1. These environments were confirmed by XRD, revealing glauconite as the prominent mineral.

Well K-A2 showed calcite and quartz significantly impeding the porosity (3%) and permeability (0.06mD). Biogenic processes are envisaged to be the primary contributor for the formation of these carbonates cements in well K-A2. Well KA-3 revealed calcite and kaolinite as pore filling minerals which primarily caused the low porosity (10%) within well K-A3 at 3880.1 m. Furthermore, the petrographic observations show mechanical compaction through quartz inclusions within albite mineral grains. Additionally, the presence of flattened quartz is

indicative of overburden pressure/compaction. Due to the presence of pore filling kaolinite flakes with relatively minor amount of albite crystals within well K-E1 (3751.61m) the porosity (10%) was reduced in comparison to the rest of the reservoir interval. However permeability remained fairly constant within the entire reservoir interval.

Quartz overgrowths, k-feldspar, kaolinite, dolomite and calcite cements exerted a profound effect on the quality of shallow marine reservoirs within the sandstones of the Orange Basin. It can be deduced that reservoirs within these shallow marine reservoirs are of poor quality.

Acknowledgments

First and foremost, praises and thanks to the Almighty, for His showers of blessings and guidance throughout my research work to complete the research successfully and for making me who I am today.

I would like to express my gratitude to the National Research Fund (NRF) for helping me with funds for my research. In addition, I am grateful to my supervisor, Dr. Opuwari of the University of the Western Cape (UWC) for his guidance and supervisory role for this research.

I owe my deepest gratitude to my parents, siblings and friends for their unconditional love, encouragement and support throughout this research period. A special thanks to my dearest friend, thank you for your perseverance, support and for being my pillar of strength throughout this challenging period.

Table of Contents

LIST OF FIGURES

List of Abbreviations

IP	Interactive Petrophysics
GR	Gamma Ray
PEF	Photoelectric Logs
mD	Millidarcies
ILD	Deep Resistivity Log
RHOB	Density Log
NPHI	Neutron Density Log
XRD	X-Ray powered diffraction
SEM	Scanning Electron Microscopy
EDS	Energy Dispersive X-ray Spectroscopy
Φ	Porosity
Sw	Water Saturation
K	Permeability
PASA	Petroleum Agency of South Africa
Na+	Sodium
K+	Potassium
Q	Quartz
A	Albite
K	Kaolinite
Ku	Kutnohorite
Ca	Calcite
P	Pyrite
G	Glauconite
K	Kaolinite
Mg	Magnesium
Mn	Manganese
Si	Silica
QC	Quartz Cement
O_2	Oxygen
Kf	K-Feldspar

Chapter 1: Introduction

1.0 Introduction

The Orange Basin which is located in Southern Africa covers approximately 3% of the African continent (nearly 37 000km^2) (PASA, 2003). The Basin is located in the Atlantic Ocean. The Basin is relatively large in which source rocks are actively producing hydrocarbon and there is potential for hydrocarbon discovery when it charges good quality reservoirs.

Porosity and permeability are two fundamental properties of sandstone reservoirs. It determines whether a reservoir is able to store and transmit commercially viable quantities of hydrocarbons. When rocks are subjected to increased depth of burial, the effects of compaction and chemical reactions between fluid organic matter and rocks will subsequently cause various minerals to precipitate (Samakinde, 2013).These minerals can either preserve porosity or cause the degradation of it by occluding, lining or bridging pore throats.

According to previous research (Samakinde, 2013; Fadipe, 2012) porosity and permeability within the Orange Basin is intensely impaired by the presence of calcite, quartz, chlorite and montmorillonite. Moreover, it has been stated that sandstones within the Orange Basin predominantly consists of quartz, calcite, montmorillonite and authigenic chlorite, hence these minerals having a major influence on the quality of reservoirs.

In light of the above, it is crucial for Exploration and Production (E&P) companies to predict the quality of reservoirs, identify allogenic and authigenic minerals as this will help define the best reservoir interval and avoid exploration failure by choosing the compatible drilling and hydraulic fluids (Jiang, 2012).

1.1 Research statement

As soon as sediments are deposited, they are subjected to biological chemical and physical forces which in due course define the type of rocks and minerals they develop. The commercial viability of a reservoir is determined by the collective effects of compaction, bioturbation, burial and chemical reactions between rocks, organic matter and fluid. It is of utmost importance to conduct integrated studies to further our understanding of reservoir sandstones and the effects minerals have on reservoir properties.

Well logs of wells KA-2, K-A3 and K-E1 in conjunction with core samples received from the PASA were subjected to several analyses. The wireline logs were interpreted using Interactive Petrophysics© and core samples underwent X-Ray powered diffraction (XRD), Scanning Electron Microscopy (SEM), Energy Dispersive X-ray Spectroscopy (EDS) and thin section analyses to reveal how the presence of minerals affects the quality of the reservoirs.

1.2 Aim and objectives

The aim of this study is to identify the effects of minerals on reservoirs, using the following: Interactive Petrophysics, core logging methods and Petrographic studies. The studies objectives are to:

- Estimate porosity, water saturation and predict permeability logs, calibrate the conventional core analysis such porosity (Φ), water saturation (Sw) and permeability (K) with the estimated parameters of porosity, water saturation (Sw) and permeability (K) from the wireline logs.
- Classify lithofacies from the cores and interpret depositional environments
- Perform XRD and SEM analysis using core samples from possible reservoirs to determine the various minerals present and subsequently analyse the highly magnified images derived from SEM. Lastly thin section analyses were conducted to identify diagenetic processes.

1.3 Outline of thesis

The present study consists of seven chapters. This section presents the general structure of the thesis. Chapter 1 provides the general information of the study, the statement of the research problem, research objectives as well as the importance of the study. Chapter 2 provides a review of studies conducted within the Orange Basin that pertains to assessing the effects of diagenetic minerals on qualitative reservoir properties using integrated approaches. The geology of the study area is outlined within this chapter.

Chapter 3 outlines the research design and methodology used in this study. In this chapter, the commonly used methods are outlined as well as the analytical tools used. This chapter explains all the methods used within this study to assess the effects minerals have on reservoirs within the Orange Basin, Offshore South Africa. It includes estimation of petrophysical parameters,

core logging and interpretation of depositional environments, XRD, SEM and thin sections analysis.

Chapter 4, 5 and 6 provides the generated results of the petrophysical properties, the geological interpretation using the gamma ray log shapes, core analysis which is described in terms of depositional environments, XRD, SEM analyses along with EDS, and lastly thin section analysis. The chapter emphasizes on how the presence of the diagenetic minerals affects the quantitative reservoir properties of the wells. In addition, chapter 4 provides the results attained from the three chosen methods, i.e. XRD, SEM, EDS and thin section analysis. In this chapter the main research findings are discussed and explanations for the results are provided. The final chapter of this study (chapter 7) delivers a conclusion based on the obtained results and suggests recommendations.

Chapter 2: Literature review

Review of key concepts and Geology of the study area

The review of the key concepts of this study is presented as follows: Firstly, it mentions the diagenetic minerals that is commonly found in sandstone reservoirs. Secondly, it described the formation of these minerals. Lastly, it describes how petrophysical properties are affected by the presence of these minerals. Further discussions are centred on the analytical tools used to identify the type of minerals present and how they affected reservoir properties. This chapter has a significant contribution towards understanding how authigenic clay minerals are formed and assessing how their presence compromises the quality of sandstone reservoirs.

2.1 The formation of diagenetic minerals within clastic reservoir sandstones

Most clay minerals are formed in the rock as a result of diagenetic processes. The most relevant diagenetic process is the dissolution of feldspar. Diagenesis can be divided into two stages. Namely, diagenesis and Late diagenesis (Ali *et al*., 2010). Diagenesis refers to processes occurring from deposition and into the shallow burial realm, for example: compaction which resulted from burial and overburden in the sediment column and is significant in fine-grained sediments. Additionally, biological/physical/chemical influence of burrowing organisms is

also one of the processes that occur during diagenesis. Once burrows are constructed within the sediment, some organisms remain in them and flush the burrows with overlying seawater, bringing about enhanced exchange between pore waters and overlying seawater.

While some elements escape the sediment through advection of pore waters as a result of compaction, many others migrate out of the sediment by diffusion, driven by concentration gradients established as a result of diagenetic processes such as mineral dissolution, bacterial degradation of organic matter and ion-exchange (Ali, Clark, & Dribus, 2010). Late diagenesis refers to processes that take place at deeper depths, during and after uplift. There are three stages of diagenesis, syn-or eodiagenesis (early diagenesis), mesodiagenesis (burial diagenesis) and epi-or telodiagenesis (diagenesis after uplift) (Ali *et al*., 2010).

There are two processes of sandstone diagenesis: physical processes and chemical processes. Physical processes occur due to compaction and pressure solution, both depending on depth of burial. Chemical processes occur due to cementation, dissolution and replacement or modification of pre-existing minerals. They usually take place in the presence of water and largely depend on salinity, the concentration of hydrogen ions in solution (pH) and the redox potential of the water (Eh).

2.1.1 Diagenetic water during the early stages of diagenesis:

Pore waters that affect sediments during the early stages of diagenesis are related to the depositional environments, which can be modified by bacterial activity and the breakdown of organic matter. Furthermore, for marine sediments, the beginning stages of diagenesis occurs with, oxidizing pore waters, which with increased depth become reducing as bacterial processes consume the oxygen.

2.1.2 Diagenetic water in deep burial:

Pore waters during deep burial are further modified by dissolution of unstable grains, reactions with detrital clay minerals, mingling with waters from other sources and precipitation of authigenic minerals. Pore waters in deeply buried sediments are alkaline, saline and neutral. The primary diagenetic processes of sandstone are compaction and pressure solution, silica and calcite cementation and lastly, clay mineral and feldspar authigenesis (Malaza, Liu, & Zhao, 2013). Compaction involved closer packing of grains and dewatering of it as a result of overburden pressure. Pressure solution occurs when the rock is fully cemented to produce sutured or irregular planes, known as stylolites (Samakinde, 2013).

Silica (SiO_2) cement is the most common type of quartz overgrowth and its precipitation occurs around the quartz grain. However, in certain instances, the boundary between the overgrowth cement and grain cannot be discriminated with the light microscope and the whole section could have an appearance of a metamorphic quartzite (Weibel & Keulen, 2008) An essential feature pertaining to quartz cementation is the fact that it is able to withstand the effects of pressure solution and compaction during later burial. Therefore, an adequate porosity will be preserved.

$CaCO_3$ cementation is essentially the earliest diagenetic cement and usually the first cements (Ali *et al*, 2010). Later quartz overgrowth and feldspar alteration is inhibited by early precipitation of calcite which results in the total destruction of permeability and porosity. On the other hand, calcite can precipitate later, postdating authigenic kaolinite and quartz overgrowths (Ali *et al*, 2010).

Commonly feldspars are altered to kaolinite and illite in sandstones. Alkaline pore waters rich in silica (Si^{4+}), aluminium (Al^{3+}) and potassium (K^{+}) are required for authigenic feldspar. These elements are sourced from dissolution of unstable grains within the sediment and from hydrolysis (Bjørlykke, 1998). The transformation of feldspar to kaolinite is the most common process to occur within the subsurface (Nelson, 2014). This process/reaction is represented by the following chemical reaction:

$$2\ KAlSi_3O_8 + 3H_2O \rightarrow Al_2Si_2O_5(OH)_4 + 4\ SiO_2 + 2K(OH)$$

Feldspar water kaolinite Quartz

For kaolinite to form, low temperatures and pressures are required. Kaolinite is either a product of weathering or it may form from ascending fluids (hydrothermal alteration of the host rock). Feldspar and muscovite are typically the parent minerals from which kaolinite forms and commonly happens-under hot-wet intertropical climates (Dolores & Cruz, 1989).

Kaolinite and illite are the most common authigenic clay minerals within sandstones (Nelson, 2014). Authigenic clay minerals occur as clay rims around grains and as pore-filling cements (Nelson, 2014). The precipitation of clay rims is often the first diagenetic event, frequently predating calcite cementation and quartz overgrowths. Illite is a hydrated authigenic phyllosilicate clay mineral, which is rich in Si, K and Al. Illite has a detrimental effect to the quality of reservoirs (Javid, 2013).

In the early stages of mesogenesis, the clay mineral chlorite forms. It continues to remain stable up until the end of the telogenesis stage (Javid, 2013). The proportion of pore-filling and pore-lining chlorite strongly changes reservoir quality. The best in terms of reservoir quality is the coarser-grained sandstones, where chlorite forms a thin pore-lining layer that does not hinder the permeability and preserves porosity (Javid, 2013). Chlorite is deposited in specific settings, namely in the transitional environments, where circulation between Fe-rich fresh waters and marine waters occurs. Chlorite-coated sandstones are frequently linked with Fe-rich depositional environments. The onset of significant chlorite growth is related with shallow or intermediate burial settings (Javid, 2013).

Albite ($NaAlSi_3O_8$) is a sodium rich mineral belonging to the plagioclase feldspar group. Albitization takes places when detrital K-feldspar or calcic plagioclase is substituted by albite. The first scenario occurs during increasing salinity of formation water. High salinity formation waters are typically dominated by Sodium (Na). This process is demonstrated by the equation below. The second scenario takes places during any stage of diagenesis as the anorthite feldspar end-member is unstable at all conditions found in sedimentary basins (Morad, Bergan, Knarud, & Nystuen, 1990).

$KAlSi_3O_8 + Na^+ = NaAlSi_3O_8 + K^+$

K-feldspar Albite

Glauconite is a green ferric-iron silicate mineral, rich in potassium (K^+) with a micaceous structure. It has a very low resistance to weathering. The occurrence of glauconite depends significantly on reducing environments. Glauconite is formed at subanoxic conditions in shallow marine environments with slow rate of accumulation and may be created by the decay of organic matter within bioclasts and faecal pellets (Javid, 2013).

2.2 Reservoir properties of sandstones

Different diagenetic minerals discussed above influence the petrophysical properties of sandstone reservoirs. Porosity and permeability are two of the most fundamental properties, as these two properties define whether a reservoir is able to store and transmit viable quantities of hydrocarbons.

2.2.1 Porosity

One of the most fundamental rock characteristics is porosity. Porosity can be represented as a dimensionless property. This fundamental characteristic is defined by the pore volume to bulk

volume ratio of a fragment of rock. There are different porosity types that are associated with the original texture of the sediment, primary and secondary porosity. Primary porosity is associated with the original depositional texture of the sediment. Secondary porosity is created after burial. Secondary porosity is typically generated through the formation of fractures, removal of cements or leaching of framework grains. In some reservoirs, secondary porosity is the predominant form of effective porosity (Ali *et al*., 2010). It is commonly referred to diagenetic porosity as it is created through the alteration of the rock.

2.2.2 Water saturation

Fluid saturation is the division of the storage volume of a rock engrossed by a particular fluid. Water saturation contains a ratio of water volume to the pore volume of the rock, where water bound clay is not taken into consideration and therefore shale corrections must be made if there is shale content within the reservoir. The portion of pore volume engrossed by a specific fluid is known as water saturation (Sw). This characteristic is expressed as 1-Sw. This is the ratio of pore volume occupied by hydrocarbons expressed as a percentage. The estimation of water saturation is carried out using the methods of effective porosity and resistivity logs. Alternative methods are used to calculate water saturation such as: Archie (1942) -used for clean sandstones. The Simandoux (1963), Schlumberger (1972), Poupon and Leveaux (1954) and the Indonesian (1968) models, these models are used for shaly sands encompassing the resistivity approach.

2.2.3 Permeability

Permeability measures the ability of a rock medium to transmit fluids. Darcy is the unit of measurement for permeability derived from Darcy's Law. This characteristic of reservoir rocks is fundamental for reservoir quality as it controls the flow direction and flow rate of the fluid accommodated by the reservoir. There are two types of permeability, namely: effective and absolute permeability. Effective permeability refers to permeability when one fluid flows in the presence of a fluid. Effective permeability is lower than the absolute permeability within a pore system because the presence of a second fluid minimizes the hole size that is available for the flow of the first fluid. Relative permeability of a rock is the ratio of effective permeability of a particular fluid to absolute permeability.

2.3 The effects of diagenetic minerals on reservoirs properties

Petrophysical evaluations of porosity, water saturation and permeability were carried out by various researchers (Kamagang 2013; Opuwari, 2010). It has been found by Kamgang, (2013)

that the porosity values within the Orange Basin ranges from 6-25% and water saturation reveal very high values of 71-86%. Furthermore, (Opuwari, 2010) encountered reservoir rocks of mainly good quality. The diagenetic processes mentioned above are the key factors that interact and consequently impact the petrophysical properties of reservoirs. Clay minerals in particular occupy pore spaces and therefore have a profound impact on reservoirs. Studies conducted by Samakinde, (2013) revealed that calcite, kaolinite and quartz cementation exerts a profound influence on the quality of reservoirs within the Orange Basin. The quartz cement either lined or filled the pore spaces. Illite on the other hand grew between pores which greatly affected permeability. In addition, study by Lombard, (2009) revealed that quartz, kaolinite, illite, calcite, chlorite and montmorillonite within the Orange Basin coat grain surfaces, block pore spaces and swells in the presence of water.

The occurrence of clay minerals are challenging to identify with ordinary petrographic tools. It therefore necessitates integration of other analytical tools, such as SEM and XRD to identify these minerals. These tools will aid to plan production strategy deduce why hydrocarbon wells are performing poorly and thereafter decide which remedial actions should be carried out.

2.4 Analytical approaches conducted by various researches

Several studies concentrated on depositional environments and stratigraphy of the Cretaceous sandstones e.g. (Samakinde, 2013), (Fadipe, 2012), (Brown *et al*., 1995). The depositional systems were identified by core logging techniques. Petrographic studies conducted by (Samakinde, 2013), (Fadipe, 2012), (Adekola, 2010) were performed to define diagenesis with regards to permeability, porosity and reservoir quality. In the current study, the aim is to analyse the morphology of minerals and their effects on reservoir properties using XRD, petrographic and SEM analysis. It has been found that the presence of minerals, especially clay minerals compromises the quality of reservoirs.

2.5 Geology of study area

Location and Stratigraphic plays present

The explored division of the Orange Basin covers 37 000 km^2 (Brown *et al*., 1995). Within the Orange Basin, three stratigraphic plays were identified, namely: Albian stratigraphic-structural, Barremian stratigraphic and Hauterivian plays. Within the past ten years, sandstone reservoir rocks in the Orange Basin had been deemed most substantial play in the South African sector of the Orange Basin recently, with emphasis on Albian stratigraphic-structural play. These

Albian aged sandstones have a detrital minerology dominated by quartz, K-Feldspar, mica and including a range of greywacke to litharenites. The diagenetic alterations on Albian sandstones, consist of feldspar and lithic fragment dissolution, compaction and reduction of the depositional porosity by means of reconstruction of grains, fragmentation and rotation of grains and cementation of quartz and carbonate. The Barremian stratigraphic play achieved its approval through the Kudu gas field offshore south of Namibia. There the gas accumulation is stratigraphically trapped in continental aeolian sandstones. A working petroleum system in the non-marine part of the syn-rift succession was established through the Hauterivian Play. The Hauterivian Play is known for being the only oil discovery in the eastern marginal graben province. The play is additionally represented by the oil that had been found. It is based in the eastern marginal province, below the Aptian transgression. The reservoir is made up of lacustrine, fluvial or deltaic sandstones. Porosity (10- 15%) and permeability (0.01-468 mD) are locally reduced by calcareous cementation and silification. Diagenesis in essences creates complications for reservoir quality. Consequently detailed analysis had been carried out, which concentrated on the diagenetic effects on reservoir properties.

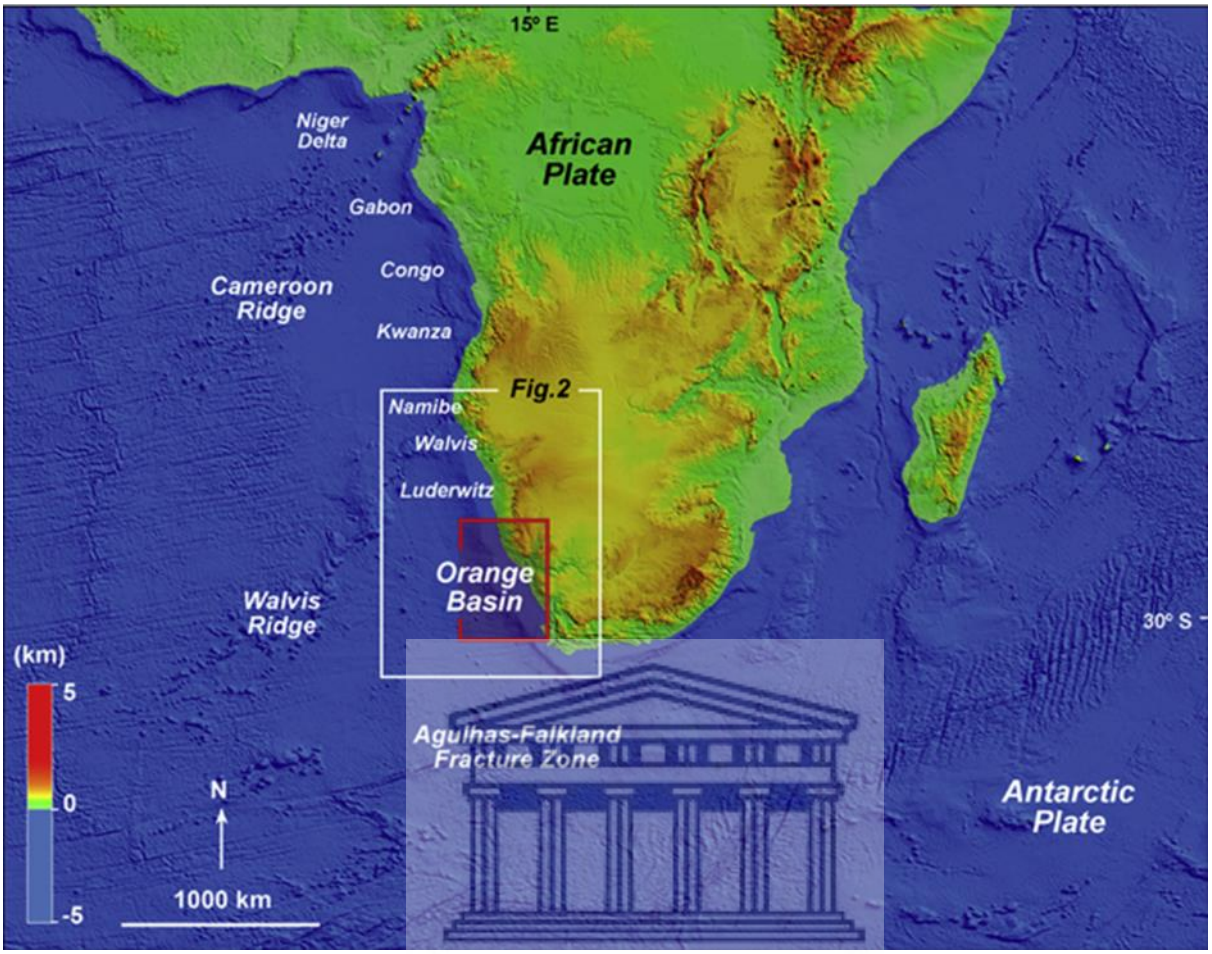

Figure 1: Location of the Orange Basin (PASA, 2003)

2.5.1 Geological overview

Beneath the Atlantic Ocean offshore from southwestern Africa lies the South African part of the Orange Basin. It extends approximately 500km from Cape Town to the South African and Namibian border. In 1974 the Orange Basin was originally explored. During this period the Kudu gas field was discovered (Yamaguchi, 2016). A substantial amount of the basin analysis study had been focused on the post-rift Cretaceous sequence stratigraphy in the basin. Between 112 and 68 Ma Soeker (PTY) Ltd concentrated on Cretaceous depositional systems. It seemed to contain possible source rocks, reservoir sandstones seals and traps within or in fault communication with the oil and gas windows (Brown *et al*., 1995).

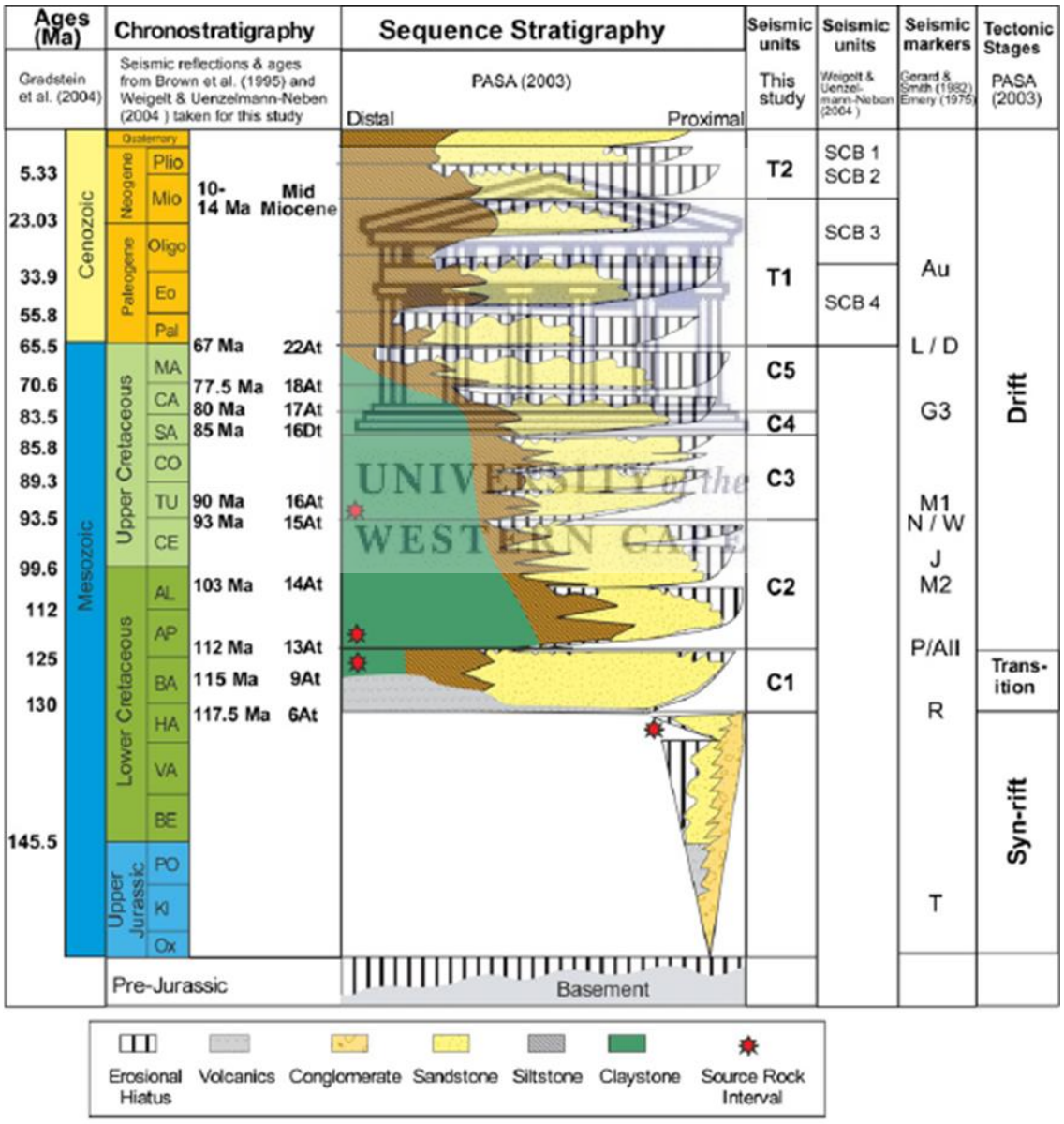

Figure 2: Sequence stratigraphic framework of the Orange Basin (PetroSA Report, 2003)

2.5.2 Tectonic setting

The Jurassic - Early Cretaceous period was followed by a sequence of rifting and drifting apart of the African and South American plates. Previously, several tectonic activities were introduced in this area, which in the latter advanced to the development of the Kalahari shield approximately 1 Ga ago when ocean-like crust was formed over the Kaapvaal Craton. The Gondwana separation resulted in the Orange Basin to experience two phases of syn-rift. The initial phase involved normal faulting during initial rifting of the Atlantic margin. These faults formed typical half-graben structures. The latter phase brought upon the deformation which was caused by the extension of drift phase sediments across the shelf.

2.5.3 Regional geology

Located offshore South Western Africa is the Orange Basin. It is situated within the passive continental margin of the South Atlantic Ocean approximately between 31 and 33.3° latitude (Brown *et al.*, 1995). The systems of the Olifant and Berg River had contributed to the sedimentation of the basin. However the influences of these river systems are restricted to the South (PASA, 2007). Margin deformation mechanisms were not active throughout most of the basin history (Brown *et al.*, 1995). Characterized by the extension and thickness of post-rift sedimentary succession deposits during the Cretaceous, the Orange Basin gradually ranges from continental east to deep marine in the west (PASA, 2007). Calcareous oozes and chemical sedimentation occur mainly of the Tertiary succession, with the wedge of drift sediments experiencing constant deformation of the paleo-shelf edges and paleo-slopes due to sediment loading and slope instability specifically occur in the Early Cretaceous.

2.5.4 Petroleum system

- Source rocks

  Within the Orange Basin source rocks occur alongside synrift upper Jurassic-Neocomian lacustrine sediments and in the shaly Lower Cretaceous deep marine sediments (Kamgang, 2013).

- Reservoir rocks

  Fluvio-deltaic and lacustrine sandstones are interbedded with conglomerates that forms the reservoir rocks of the basin. Deposited during the Early Cretaceous deep marine,

reservoir rocks were additionally deposited during the post-rift succession. The premier oil bearing reservoir is located within the Albian succession and contains thick as well as thin-bedded clay-silt and sand sequences (Kamgang, 2013).

- Traps

Both stratigraphic (pinch out and dome) and structural (fault closures) structures assists in the trapping of hydrocarbons within the Orange Basin (Broad & Mills, 1993).

Chapter 3: Research methodology

Research framework

Figure 3 below, shows the research design used to integrate and articulate the procedures and analytical steps adopted to address the research problem of this study. The research design and methodology includes estimation of petrophysical parameters, core logging and interpretation of depositional environments, XRD, SEM and thin sections. A combination of desktop work and laboratory work has been applied to this research.

3.1 Estimation of petrophysical parameters

The petrophysical data for wells K-A2, K-A3 and K-E1 were provided by PASA. The petrophysical data, that is porosity, water saturation (Sw) and permeability (K) shall be interpreted using the petrophysical software, Interactive Petrophysics©. The conventional logs such as the gamma ray log (GR) was used to identify lithology, neutron (NPHI) and density (RHOB) were used as a supplementary method for deducing porosity, and resistivity log (ILD) was used to identify saturation of fluids. However, photoelectric (PEF) logs were not available and therefore better mineralogy and clay type interpretation was limited.

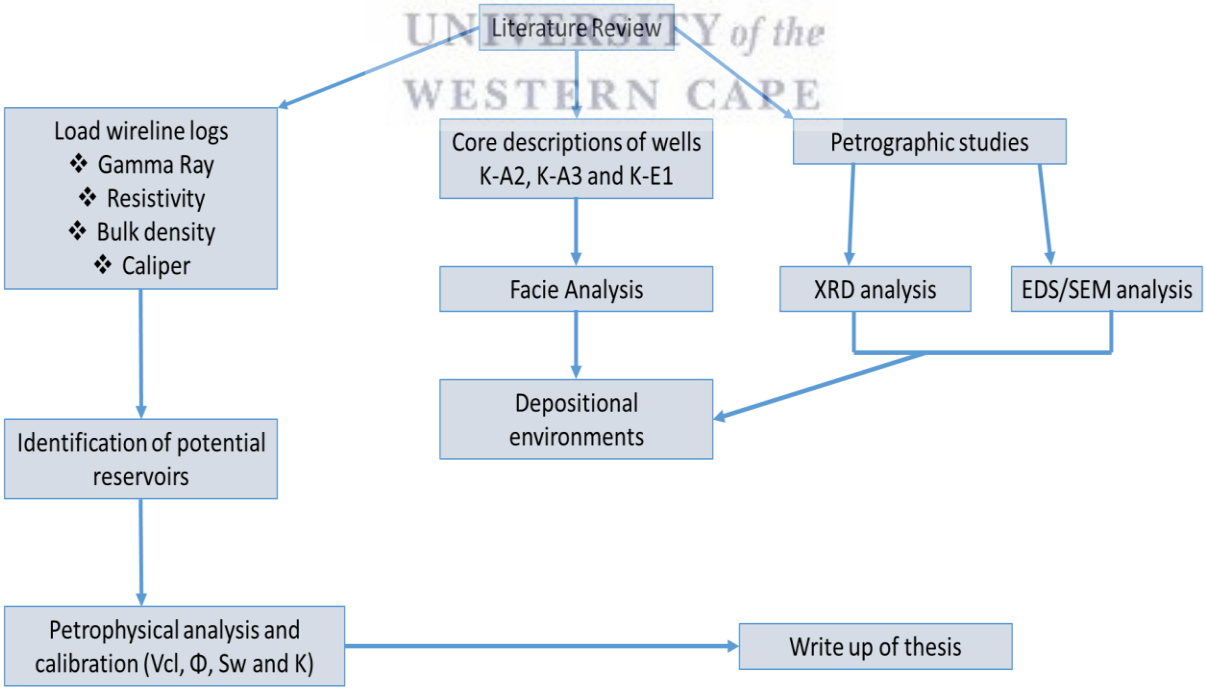

Figure 3: Flow chart of methodological process

3.1.2 Net/Gross

The reservoir thickness was determined by defining a basis for reservoir and non-reservoir sands utilizing a Gamma ray log. This was managed by assigning a baseline on the gamma ray log.

3.1.3 Shale and Clay Volume

A favored method to linearly calculate the volume of clay is the gamma ray method. This is due to its response to radioactive materials. Moreover, the linear gamma ray method in infamous to overestimate the volume of clay, producing a pessimistic synopsis. Thus there are numerous other types of gamma ray models to estimate volume of shale. These are: the Larionov model (1969) for older rocks, the Clavier model (1977), the Stieber (1975) model and the Larionov model for Tertiary rocks. The model most suitable for the current study is the Stieber model, which is commonly used for shaly sands. It produces the least amount of clay within the sandstone intervals (Dejtrakulwong *et al*., 2009).

Gamma ray method:

IGR= (GRlog-GRmin) / (GRmax-GRmin)

Where:

IGR= Gamma ray index

GRlog = Gamma Ray Log reading of formation

GRmin = Gamma Ray Matrix (clay free zone)

GRmax = Gamma Ray Shale (100% clay zone)

Stieber method:

VclGr = Z/1+STB (1-Z)

Where:

Z = VclGr linear

STBC = VclGr linear

3.1.4 Porosity

A density-neutron log was utilized to calculate the total porosity as shown in equation 2

Φ= (ðma - ðb)/ (ðma – ðfl)

Where:

Φ = porosity derived from density log

ðma = matrix density

ðb = bulk density (includes porosity and grain density)

ðfl = fluid density

Additionally, the neutron density and sonic model was used to calculate porosity for wells K-A3 and K-E1.

3.1.5 Water Saturation

The Simandoux (1963) and Indonesian models (1968) is proven to be suitable for this study. The calculations for these models are layed out as:

Simandoux:

1/Rt = Φ^m * Sw^n / a*Rw + Vcl * Sw/Rcl

Where:

Rt = Input resistivity curve

Sw= Effective water saturation

m = Cementation factor

n = Saturation exponent

Rw = Formation resistivity water

Vcl = Wet clay volume

Rcl = Resistivity of the clay

Indonesian:

$1/\sqrt{Rt} = (\sqrt{\Phi}^m / a*Rw + Vcl^{(1-(Vcl/2))} / \sqrt{Rcl}) * Sw^{n/2}$

Where:

Rt = Input resistivity curve

n = Saturation exponent

3.1.6 Permeability

Darcy is the unit of measurement for permeability, acquired from Darcy's law. The theorem for Darcy's law is:

$Q=K (P_1-P_2) A/\mu L$

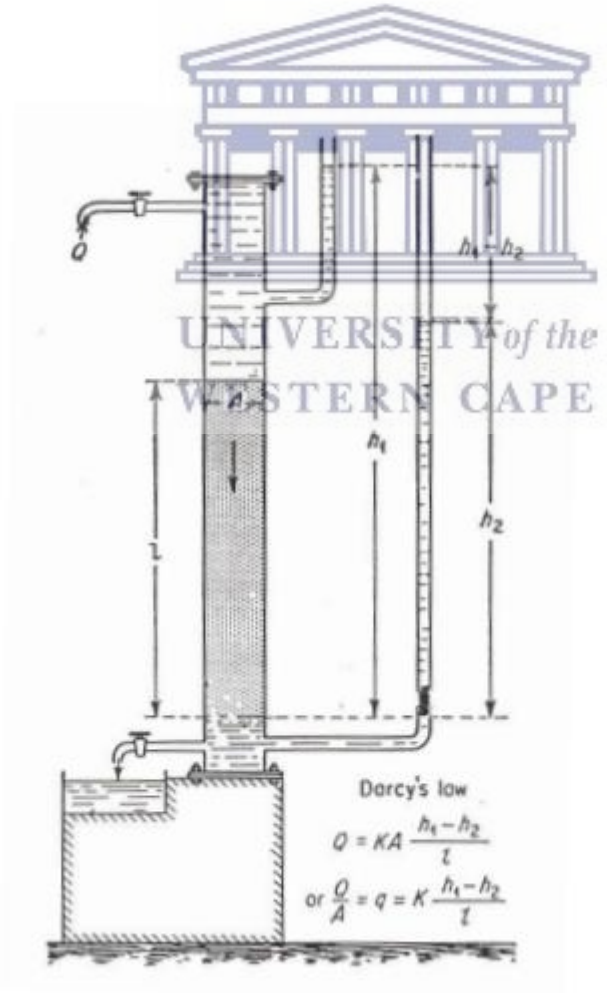

Figure 4: Darcy's experiment on flow of water

Where:

Q= rate of flow

K= permeability

(P_1-P_2)= Pressure drop across the sample

A= cross-sectional area of the sample

L= length of the sample

μ= viscosity of the fluid

The permeability can be predicted from various models and then calibrated with core data (derived from Darcy's law) to determine the best fitting model. The model used within the study is as follows:

The Wyllie and Rose method:

K = a * (Φ^c / Swir^c)

Where:

K= permeability

Φ= porosity

Swir = irreducible water saturation

Swir is calculated as follows:

Kbuckle = PHIe * Sw

Swir= Kbuckle/PHIe

Parameters are used differently for each individual researcher as stated below:

Researcher	CPERM (GAS)	DPERM	EPERM
Morris-Biggs	6500	6	2
Timur	340	4.4	2

Table 1: Parameters applied within study

3.2 Depositional Environments

Core logging in conjunction with gamma ray logs were used to confirm depositional environments. Funnel, cylindrical, serrated and bell shapes are exhibited by the gamma ray log response, as shown in figure 5. Theses shapes are indicative of the depositional environment of the rock.

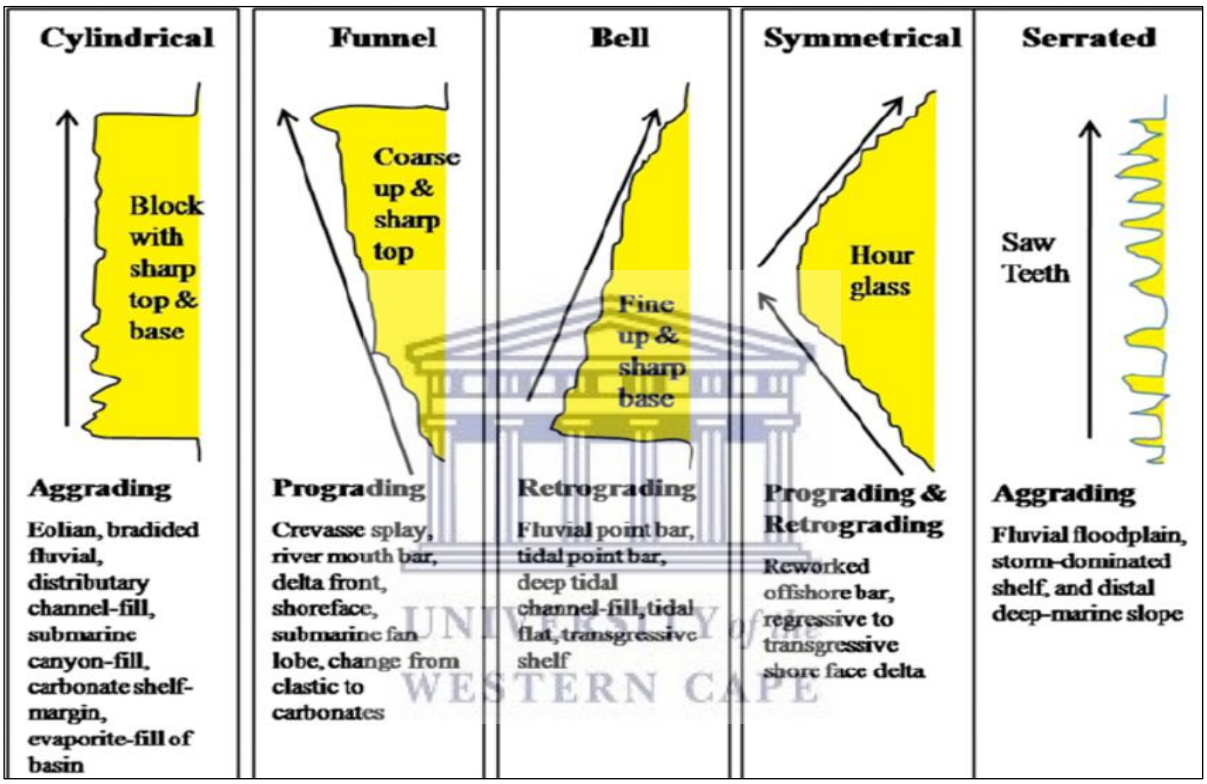

Figure 5: Correlation between facies and logs shapes (SEPM. & Geology, 2013)

3. 3 X-ray Diffraction (XRD) analysis

Phase identification of a crystalline mineral is commonly analyzed using XRD. The X-ray diffractometers are composed of three elements: X-ray detector, X-ray tube and a sample holder. Cuttings from different depths of the cored intervals was crushed to a powder form of approximately 0.5g and then used as the input for the XRD analysis.

3.4 Scanning Electron Microscopy (SEM) and Energy Dispersive X-ray Spectroscopy (EDS) analysis

A variety of signals are generated at the surface of solid specimens by a beam of high energy electrons. The resulting signals expose information about the specimen, including orientation

of minerals making up the sample, crystalline structure, chemical composition and external morphology. The derived spectrum is used to validate the analysis of petrographic studies. Moreover, the high resolution images obtained is used to identify how minerals within the Orange Basin affects the reservoir quality. EDS is an analytical method that can be used in conjunction with numerous electron-beam based techniques, such as SEM. EDS was used to analyse the elemental composition of individual points.

3.5 Thin section analysis

Thin sections delivers samples for visual study of textural properties and processes that may have affected the rock (depositional and diagenetic activity). They also allow for mineral identification and abundance. The thin sections were derived from core samples of potential reservoir sandstones.

Chapter 4: Results

Results

4.1 Log characteristics of wells K-A2, K-A3 and K-E1

The electrical logs for wells K-A2, K-A3 and K-E1 within the Orange Basin were examined. The motive for geophysical log interpretation is to deliver substantial information about the geological and physical conditions in the subsurface.

4.1.1 Log interpretation of well K-A2

Borehole K-A2 was drilled 3 km south-south west of the original well (K-A1) in order to further evaluate the hydrocarbon potential of the K-A prospect which is situated in the central Orange Basin, 130 km west-north-west of Saldanha Bay, South Africa.

Two cores were recovered, however only Core 1 was available for analysis. Core 1 comprised of the Lower Cretaceous sandstones, ranging from 3976.9 m-3989.7 m and consisted of tight to slightly porous silty sandstone interbedded with shale and siltstone.

A baseline, 80 API was chosen for the gamma ray log (track 2 on figure 6) to differentiate between sandstone and shale. The lowest gamma ray reading for sandstone intervals was 44 API (American Petroleum Institute) is the largest U.S. trade association for the oil and natural gas industry, whilst the highest gamma ray reading was 77 API for shaly sands. Track three represents deep resistivity (ILD) and spherically focussed resistivity logs (SFLU). These logs measured the resistivity of the wells. Formation resistivity (Rxo) measured the flushed zone resistivity and was directly read from SFLU and therefore the SFLU log displayed a slightly higher resistivity than ILD due to the flushed zone consisting of mud filtrate and residual hydrocarbons.

Figure 6 displays no evidence of hydrocarbons as the resistivity log shows no pronounced spikes. Track four represents NPHI (neutron porosity) and RHOB (density) logs. RHOB was used as the input for porosity calculation. The upper part of the reservoir (3978.4 m-3981 m) consists of a higher porosity (19%) than the lower reservoir interval (3988.61 m-3991.21 m) which consists of an average porosity of 5%. The Indonesian method, (1971) was used to estimate the water saturation within the well due to the fact that the sandstones reveal a shaly sandstone nature. The Indonesian best matches the Sw routine core analysis. The upper

reservoir interval (3978.2 m- 3983.4 m) has an average water saturation of 54%-63% whilst the reservoir lower interval (3985.6 m-3990.9 m) has an average water saturation of 67%-93% which signifies that the reservoir is mainly water saturated. The water saturated reservoir is accompanied by low porosity and permeability. The Wyllie-rose model, (1950) was applied to predict the average permeability. The permeability ranges from 0.001-1.30 mD. The parameters used are based on Timur, (1968) which proved to be reliable as it calibrated well with the core data.

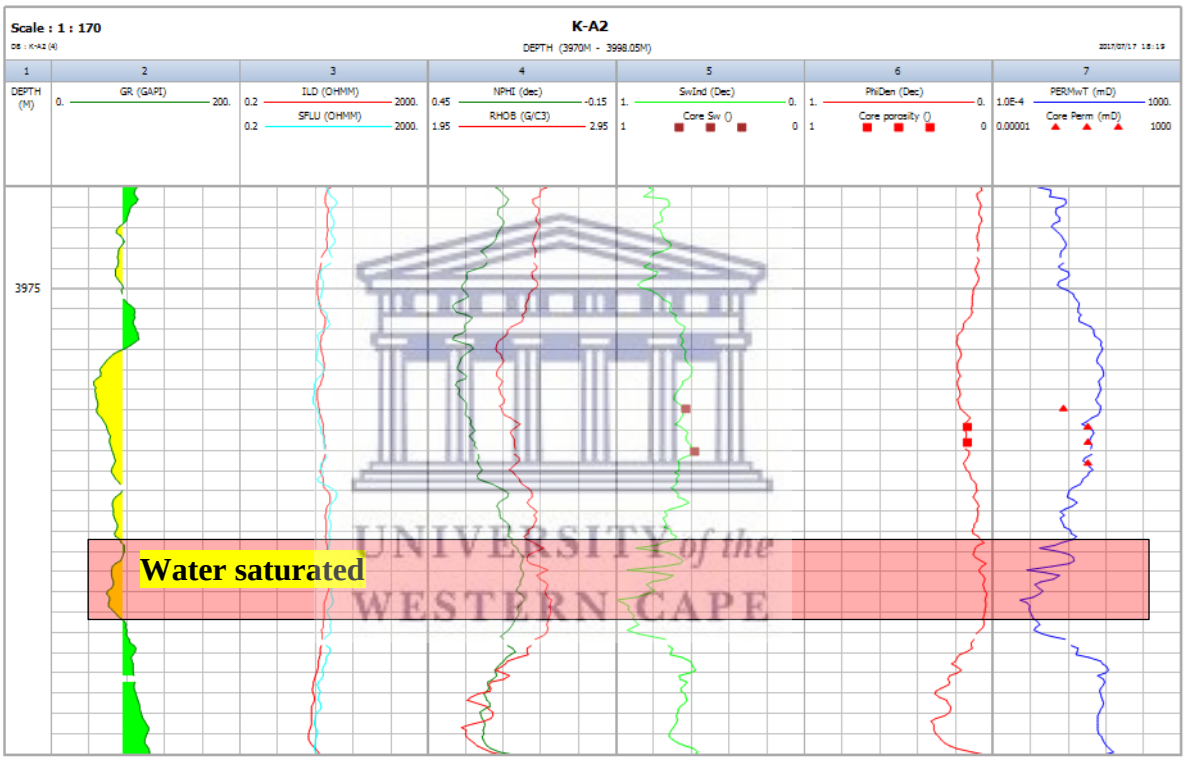

Figure 6: Log interpretation of well K-A2

4.1.2 Log interpretation of well K-A3

Gamma, ILD, RHOB and NPHI logs were spliced in order to form a single continuous curve. A baseline of 60 and 70 API was used for core 1 and core 2 to distinguish between sandstone and shale, respectively. The gamma ray log displayed the cored sections ranging from a depth of 2906 m-2914 m for figure 7 and 3875 m-3884 m for figure 8, predominantly consisting of sandstone. The ILD displayed fairly low values for both cores, suggesting that the sandstone reservoir could mainly be water saturated. Porosity log displayed an average porosity of 10%-16% for core 1 and 9%-17% for core 2, since the core data fitted reasonably well with the porosity estimation, the neutron density estimation was regarded as a reliable source for the estimation of porosity (track six). The Indonesian shaly sand, 1971 was used to calculate water saturation for core 1 and 2. Core 1 revealed a Sw between 56%-87%, whereas core 2 revealed a Sw between 31%-39%. These values imply that the upper reservoir interval is mainly water saturated. The well completion reports stated an average water saturation of 75% for the core 1 interval and therefore the Indonesian method was more acceptable (track five). The permeability curve was not included due to the poor relationship between the core and petrophysical data.

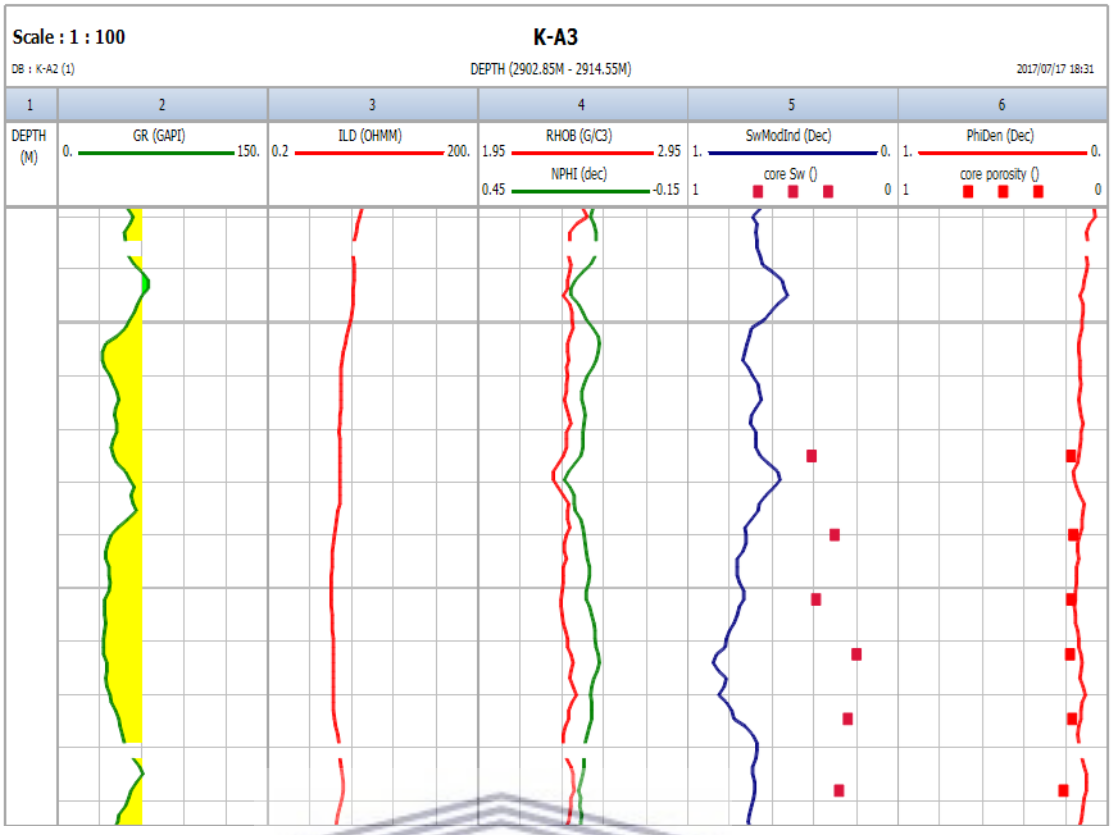

Figure 7: Petrophysical properties of well K-A3, displaying core 1

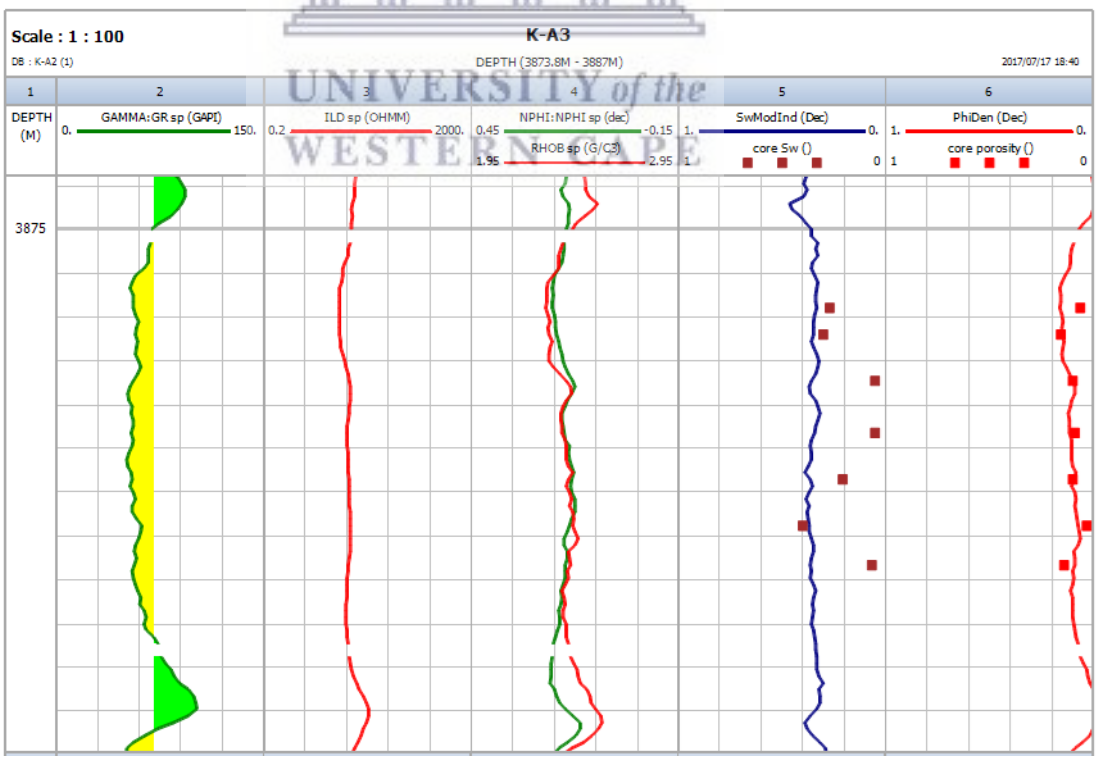

Figure 8: Petrophysical properties of well K-A3, displaying core 2

4.1.3 Log interpretation K-E1

Borehole K-E1 was drilled in 323m of water depth in order to test for hydrocarbons in the K-E synsedimentary-fault play prospect located in the Orange Basin, 180 km off the west coast of South Africa.

A baseline of 30 API was used for well K-E1. The sandstone interval ranges from 3747.5 m-3753.9 m, which consist of interbedded sandstone and shale layers. The peak displays by the resistivity log in track three, figure 9 indicates the presence of hydrocarbons and is further authenticated by the gas effect shown by the neutron and density crossovers in track four. The resistivity peaks at 9.57 ohm and is indicative of the gas effect as hydrocarbons have a higher resistivity than water. Sw was estimated using the Indonesian method and ranges between 31%-81%. The porosity ranges from 3%-16% and was calculated using the sonic method as this method fitted the core data well. A slight decrease in porosity was noted at depth 3751.76 m, this drop in porosity could be attributed to the presence of clay minerals. Furthermore, the permeability ranged from 0.001-1.30 mD which was calculated using the Wyllie rose model (track seven).

The porosity calculations revealed a range of 3%-18% for well K-A2, 2%-13% for well K-A3 and 3%-16% for well K-E1. The permeability's ranges from 0.08-0.1 mD and 0.001-1.30 mD for K-A3 and K-E1, respectively. Thus, the findings of the petrophysical evaluation of the wells in Interactive Petrophysics indicate that the reservoir intervals of wells K-A2, K-A3 and K-E1 are of poor to good quality. Based on the core analyses in chapter 4.2, the depositional environment is mostly shallow marine, specifically tide dominated for well K-A2, sandstone channel for well K-A3 and intertidal environment for well K-E1. These environments were confirmed by XRD, revealing glauconite, pyrite and calcite as prominent minerals.

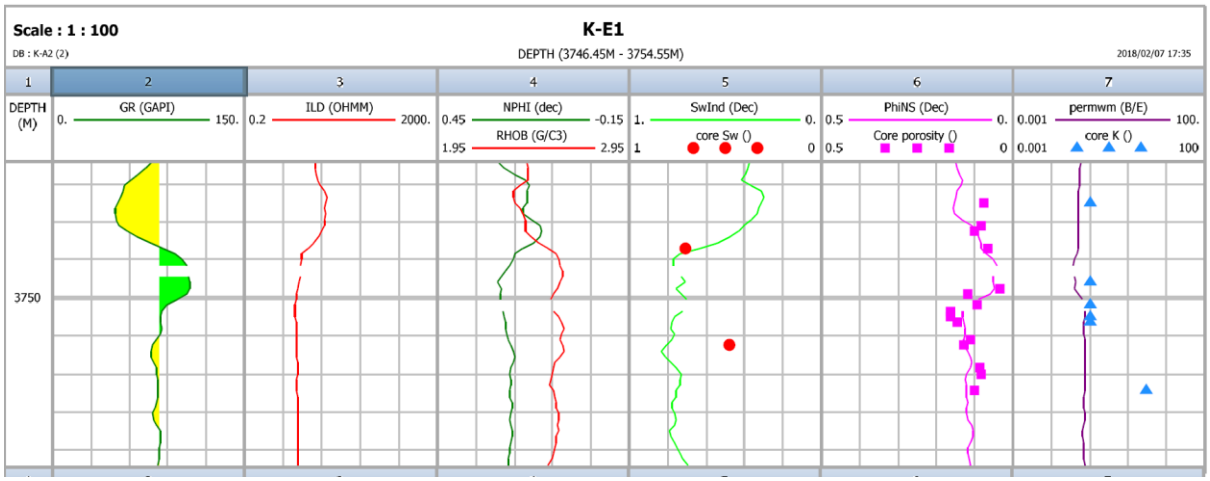

Figure 9: Petrophysical properties of well K-E1

Key insights from the reviewed literature

Interactive Petrophysics© software was used to calculate the three main reservoir properties, porosity, water saturation and permeability. The calculated results were compared to the core analysis; however, an insufficient amount of core data was available.

Well KA-2 reservoir interval ranged from 3976.9 m-3989.7 m and displayed a funnel motif in the gamma ray logs. Porosity ranged from 3%-18% and was calculated by using RHOB. An average Sw of 67% and average permeability of 0.44 mD was estimated. The core data fitted quite accurately with the generated results and therefore these input parameters were acceptable.

Well K-A3 was spliced in order to form a single continuous curve. The neutron sonic method was used to calculate the porosity and consequently generated an average porosity of 13% for core 1 and 11% fore core 2. The Indonesian method served as the input for water saturation and resulted in a water saturation of 73% for core 1 and 35% fore core 2. However, there was a variance in the core and well log data, this variance indicated that the Indonesian shaly method as well as the other stated methods was not accurate in calculating water saturation.

Well K-E1 reveals an average water saturation of 60% which was estimated using the Indonesian method. The porosity and permeability were considerably lower than wells K-A2 and K-A3, as they ranged from 3%-16% and 0.001-1.30 mD respectively.

4.2 Core Analysis

The facies of wells K-A2, K-A3 and K-E1 are described in terms of depositional environments. These wells are described by detailed description of the facies, recording all the characteristics of its lithology, sedimentary structures and texture. The identification of the sedimentary facies is crucial for the reconstruction of sedimentary environments.

4.2.1 Core 1 of well K-A2

Very fine-grained sandstone, siltstone and shale characterize core 1 of well K-A2. The base of core 1 (3991.54-3991.18 m) is characterised by interlaminated shale and siltstone which fine upward into light-medium grey sandstone, angular to round grains and consists of lignite fragments. A well-defined large burrow distorting lamination features are visible at 3989.99 m.

Shell fragments, calcareous and carbonaceous sandstones, shale clasts (deformed in places), parallel lamination, bioturbation, ball and pillow structures and emerging flaser bedding became more dominant with depth along with abundant shell fragments that effervescence in the presence of hydrochloric acid. A parallel layer of dolomite occurred at 3988.61 m and flame structures are apparent at 3987.98 m. Climbing ripples and well defined wavy laminations of shale are evident at 3986.50 m.

Furthermore, bioturbated sandstone and mudstone are fairly widespread throughout the core and comprised of balls and pillow structures. Load cast features are observable with interlaminated shale and siltstone forming wavy laminations and ripples.

Carbonaceous sandstone containing lignite fragments is present, furthermore calcite filled fractures were identified by the effervescence of hydrochloric acid. This bed was overlain by carbonaceous shale marking a sharp contact at 3984.29 m. Parallel laminations are observed at depths between 3984.10-3984.29 m with minor burrows and bioturbation present.

The uppermost interval of the core from 3981.90-3984.29 m consisted of calcareous sandstone that are well sorted and very fine grained which grade to a darker grey sandstone at 3982.20m due to the presence of lignite fragments.

Interpretation

A coarsening upward sequence, the abundance of silt, silty sand, lignite, compaction, climbing ripples, dewatering structures and grain flow structures such as ball-and-pillow are indicative of delta-front deposits (Boggs, 1987).

The parallel laminations are an indication of rapid flows that formed during deposition occurred in the upper bed flat field of the upper flow regime. These flows are possibly turbidity currents. The deposits were emplaced as gravity flows due to the absence of storm generated deposits (hummocky and swaley cross-stratification).

Sparse bioturbation at the top of the succession indicates suppressed biogenic activities attributed to the highly stressed environment activated by temperatures and fluctuating salinities combined with a huge amount of suspended sediment load and quick deposition (Oyanyan & Oti, 2015). Bioturbation played an important role in altering the porosity and permeability within fine grained sandstone units as it generated sand filled burrows and destroys primary sedimentary structures. Bioturbation is therefore a fundamental source of reservoir heterogeneity. This effect can be clearly seen when analysing the porosity log. Porosity tended to be higher in intervals in which bioturbation is sparse as compared to where bioturbation is more dominant (Gringas, Pemberton, & Smith, 2015).

Load-deformation features and ball and pillow structures evidence early soft sediment deformation processes. These features resulted from the instability of sediments and density contrasts between rapidly deposited sand, clay and silt.

Evidence of water escape structures are formed by the deformation of liquefied material caused by the rapid release of excess pore pressures due to loading by overlain deposits or seismic shocks which altered the sedimentary fabric. Such release of excess pore pressures eventually distorts the original layering as flame structures.

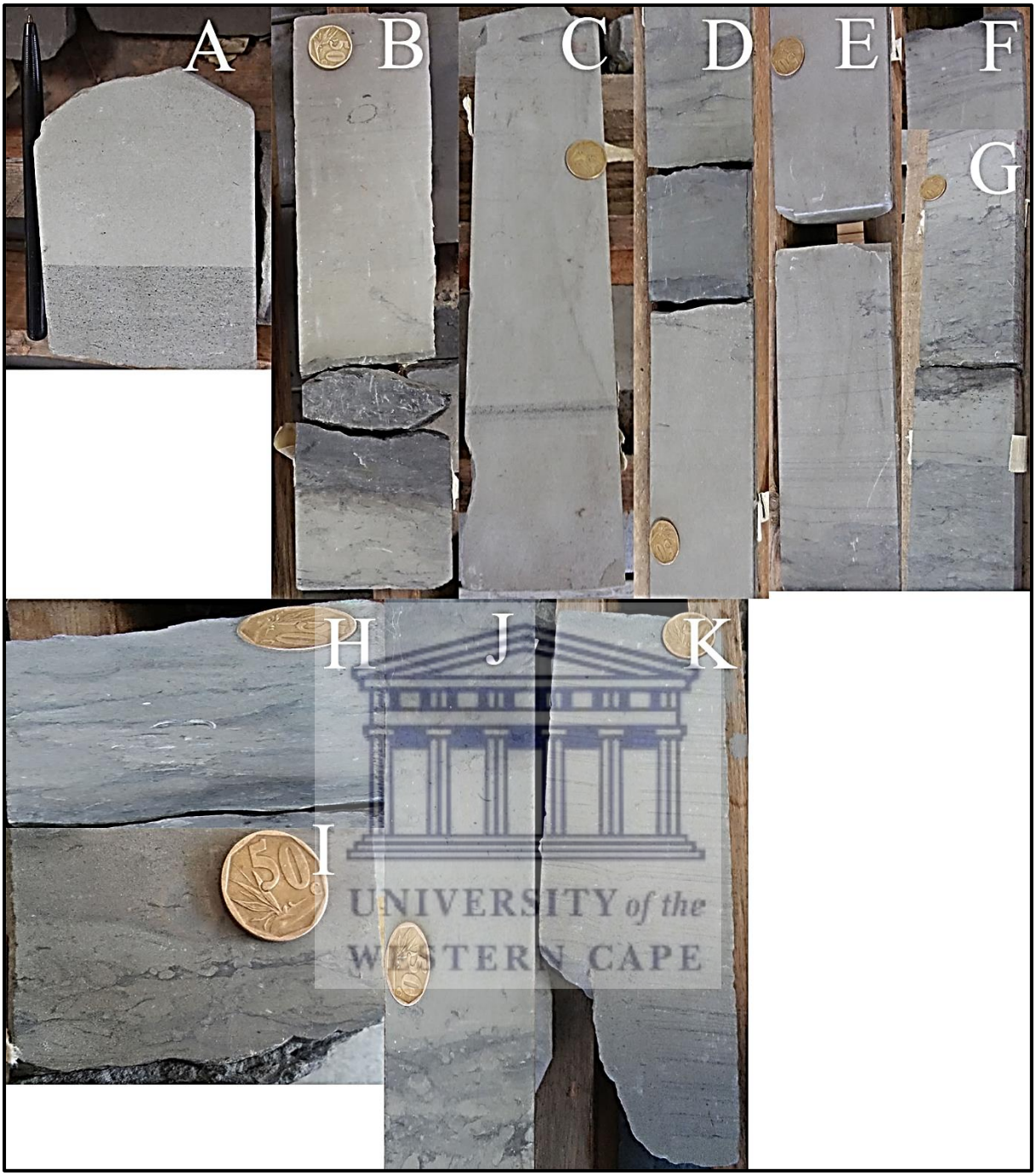

Figure 10: A~ 3981.90-3982.20m, very fine-grained sandstone. B ~ 3982.20-3984.29m, amalgamated sandstone. C~ 3984.37-3984.66m, fine grained sandstone. D ~ 3984.86-3985.10m, siltstone grading into shale. E ~ 3985.10-3985.50m, fine grained sandstone. F ~ 3985.55-3985.75m, siltstone. G ~ 3985.95-3986.70m, siltstone and shale. H ~ 3987-3987.31m, siltstone and shale. I~ Flame structure at 3987.98m. J ~ 3988.60-3989m, medium grey siltstone. K- 3990.70-3990.70m, finely interlaminated shale and siltstone.

4.2.2 Core 1 of well K-A3

The cored (2906-2914.5 m) interval was dominated by medium-very fine-grained sandstone and coarse siltstone beds. The base of the core (2914.35-2912.66 m) was characterised by homogenous fine grained sandstone, comprised of quartz with no apparent sedimentary features. Overlying this interval are heterolithic laminations of sandstone and claystone. These heterolitic laminations included flaser to low angle bedding with prominent mud drapes towards the top. Rip-up mud clasts of various sizes (elongated) within fine grained sandstones are observed from a depth of 2909.99-2910.94 m, with them becoming more pronounced in the upper part. Fine grained sandstone with planar lamination and low angle cross bedding are observed with decreasing depth. Fining upward into very fine grained sandstone/coarse siltstone with a pronounced shale streak of 0.3mm in width at a depth of 2908.83 m. This bed coarsenes upward into fine-medium, light grey sandstone and displaying discontinuous shale bedding with interlaminated clasts.

Interpretation

The heterolithic laminations allow interpreting core 1 as intertidal deposits or tidal bar deposits (tide-dominated sequence). Gamma ray logs with relatively constant gamma ray readings suggest a tide dominated environment (Siddiqui, EL-Ghali, Rahman, Mijinyawa, & Ben-Awuah, 2013).

The flaser bedding present could be the result of ripple bedding with numerous mud flasers/drapes. This structure described by Reineck & Singh (1980) implied both sand and mud were available and that periods of current activity alternated with periods of quiescence. During periods of current activity, the sand was transported and deposited as ripples, while the mud was held in suspension. When the current subsided, the suspended mud settled into the troughs and over the ripples. During reviving current flow the previously formed current ripple crests are eroded and the next layer of sand was deposited.

Flaser bedding was formed in an environment in which conditions for deposition and preservation of sand were relatively more favourable than for mud. Moreover, the presence of mud drapes is also an indicator of a tidally influenced environment. There would be a short period in which there was no flow during which time the current changes direction at high or low tide. The load that are held in suspension are deposited as a thin layer of mud. When the current became more strong during the next tide, the mud layer previously deposited will not

be removed as the clay rich sediment is cohesive and was more resistant to erosion (Nichols, 2009).

4.2.3 Core 2 of well K-A3

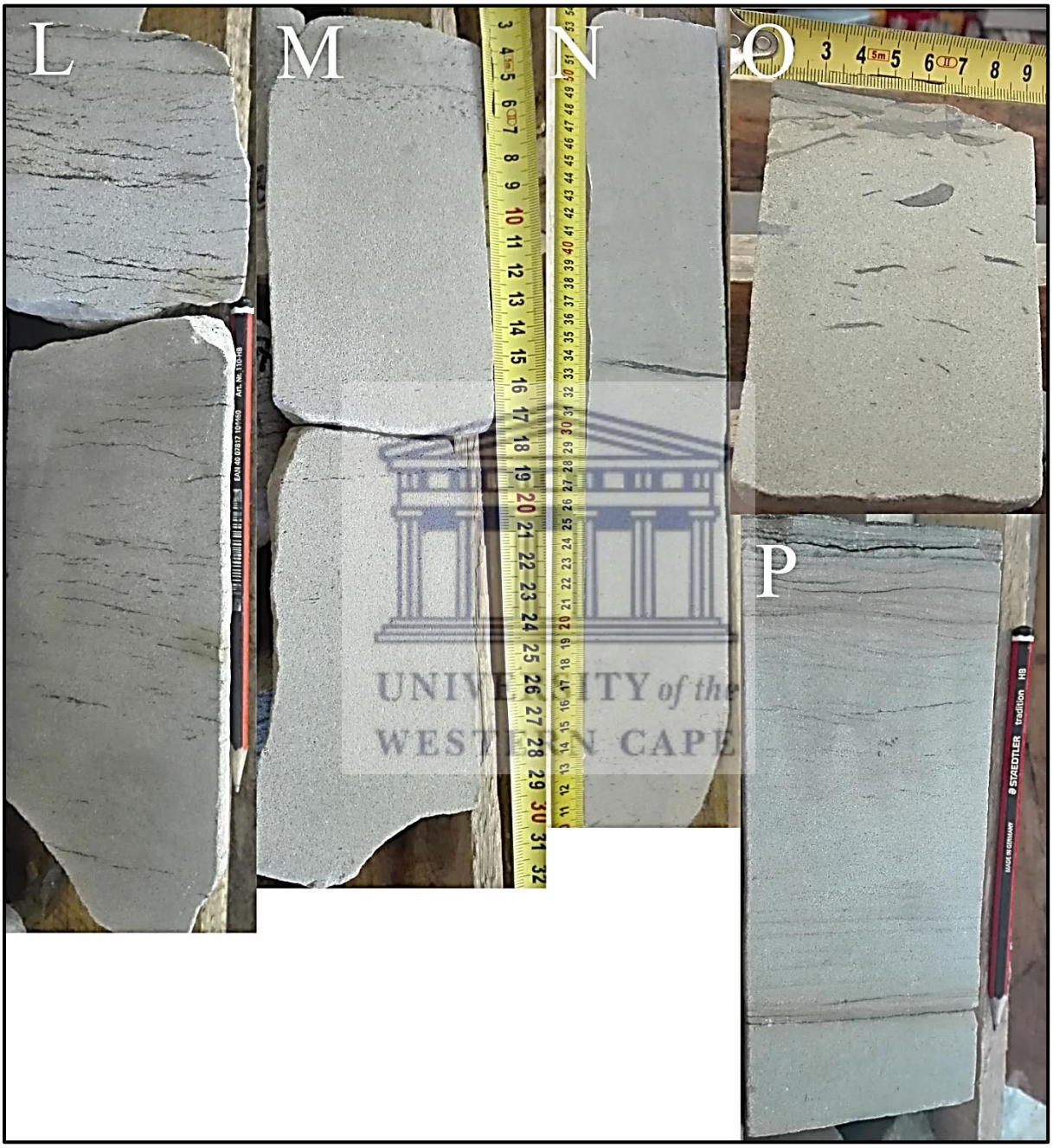

Figure 11: L ~ 2906.50-2907.28m, light-medium grained sandstone. M ~ 2907-2908.05m, fine grained sandstone. N ~ 2908.05-2909.15 m, coarse siltstone. O ~ 2909.99-2910.82m, fine grained sandstone, P ~ Fine grained sandstone.

Core 2 was characterised by light-medium grey, sub rounded to rounded calcareous sandstones with dolomite nodules, angular shale clasts in places and little to no glauconite. Very fine

grained sandstone, consisted of quartz and pyrite alternating with planar laminations within fine grained sandstones. Highly bioturbated shale laminae with alternating sandstone layers commenced at a depth of 3879.15 m and continued to a depth of 3878.90 m which subsequently graded into light-medium grey, very fine grained calcareous sandstone. The sandstone was fairly well sorted with shale clasts in places.

Interpretation

The presence of massive sandstone, planar lamination and bioturbation implied a deposit in a sandstone channel on an outer shelf. The sandstone units contained planar bedding that are indicative of high energy turbulent flow. According to Stone *et al* (2005), the shale clasts are most likely consolidated shale substrate that were ripped up, transported and ultimately redeposited within the body of the current transported sediment.

4.3.3 Well of K-E1

The cores in well K-E1 are characterised by light grey, argillaceous as well as carbonaceous fine grained sandstone and shale intervals. Fine grained, argillaceous and carbonaceous sandstone, sub angular-sub rounded in nature with glauconite in places was noted from depth 3751-3752.40 m. Flaser, and wavy, lenticular bedding was fairly dominant throughout the core. Low angle cross bedding as well as planar laminations became apparent with decreasing depth.

Interpretation

The presence of flaser, lenticular and wavy bedding alternating with argillaceous intervals and the occurrence of rip up mud clasts in certain places are indicative of an intertidal depositional environment. These features are associated with constantly fluctuating but reasonably low energy conditions with transitory periods of sand bedload transport by tidal currents and wave action alternating with fine sediment deposition from suspension.

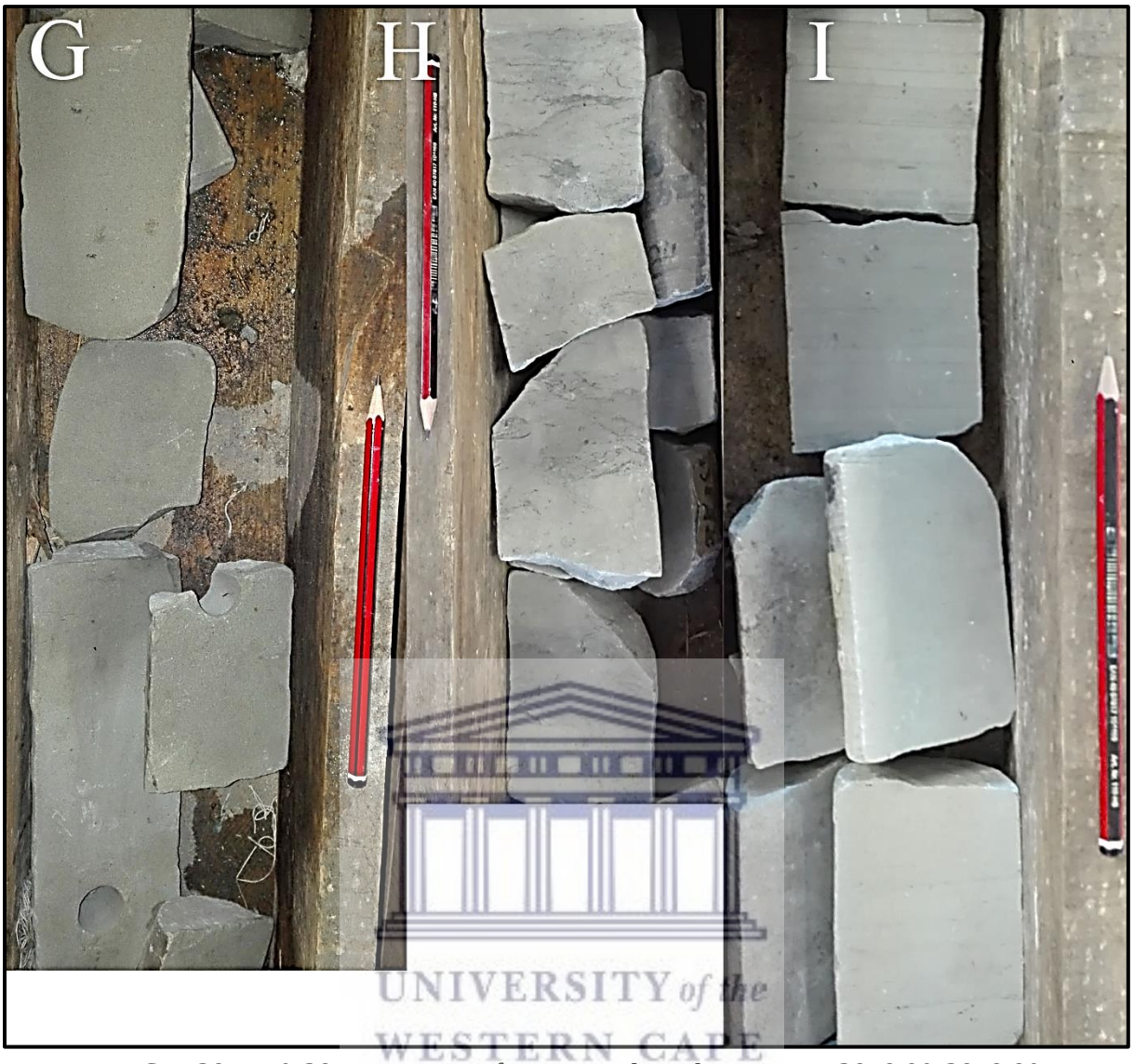

Figure 12: G ~ 3875.50-3877.21m very fine grained sandstone. H ~ 3878.90-3878.80m very fine grained sandstone and biouturbated mudstone laminae. I ~ 3879.15-3879.98m Very fine grained sandstone.

Key insights from the reviewed literature

Well K-A2 displayed a coarsening upward sequence along with abundant silt and silty sand. Its calcareous nature and abundance of shell fragments are indicative of a shallow marine environment. The presence of climbing ripples, laminations and burrows aids in the confirmation that the cores of well K-A2 were deposited under shallow marine conditions.

The cored section of core 1 of well K-A2 (2906-2914.5m) was dominated by medium-very fine-grained sandstone and siltstone beds. The presence of prominent mud drapes and flaser bedding served as an indicator that the sand body were influenced by a tidal environment. The

identification of pyrite was indicative of sulphate and organic matter, which often occurred in marine sediments

The presence of planar bedding in core 2 of well K-A3 are indicative of high energy turbidity flow. Additionally, the massive sandstone units represents a deposit of a sandstone channel.

The prominent sedimentary structures identified in well K-E1 are flaser, lenticular and wavy laminations. These features are a result of fluctuating but low energy conditions and therefore suggested an intertidal environment.

XRD analysis

Well K-A2

The presence of albite in both samples (see figure 13 and 14) suggests the influence of meteoric waters. The process is known as albitization. K-feldspar reacted with Na^+ from the meteoric waters which resulted in the formation of Albite and released K^+ (Mohabbat, 2012). This reaction is demonstrated below:

(K-feldspar) 2 $KAlSi_3O_8 + Na^+ \rightarrow$ (Albite) $NaAlSi_3O_8 + K^+$ ……..equation 1

Furthermore, the formation of kaolinite was linked to the dissolution of k-feldspar/plagioclsse or micas (Bjorlykke, 1996). These reactions are shown below:

(Feldspar) $2K^+$ (Na^+) $AlSi_3O_8 + 2H^+ + 9H_2O \rightarrow$ (Kaolinite) $Al_2SiO_3(OH)_4 + 2H_4SiO_4 + 2K^+$ (Na^+)…….equation 2

This reaction occurred under acidic conditions associated with continuous influx of meteoric water.

(Albite) $2NaAlSiO_8 + 9H_2O =$ (Kaolinte) $AlSi0_2O_5 + 4H_4SiO_4 + 2Na^+$ ……equation 3

Kutnohorite is a calcium manganese carbonate mineral rich in magnesium and Iron. The Mn was likely derived from metamorphic rock, whereas the Mg suggested that the rock at some time came into contact with hydrothermal fluids rich in ferromagnesiun minerals.

Based on the research of Waderhaug & Bjorkum, 1998, it can be suggested that the source of calcium was mainly derived from biogenic carbonate within the rock. This can be substantiated by the presence of abundant fossils in Core 1 of well K-A2. The dissolution of carbonate shell

fragments might have provided the ions for calcite precipitation. The source of iron for the formation of pyrite is thought to be due to the reduction of detrital iron oxides in an environment rich in organic material and this could be related to the carbonaceous material identified in the core.

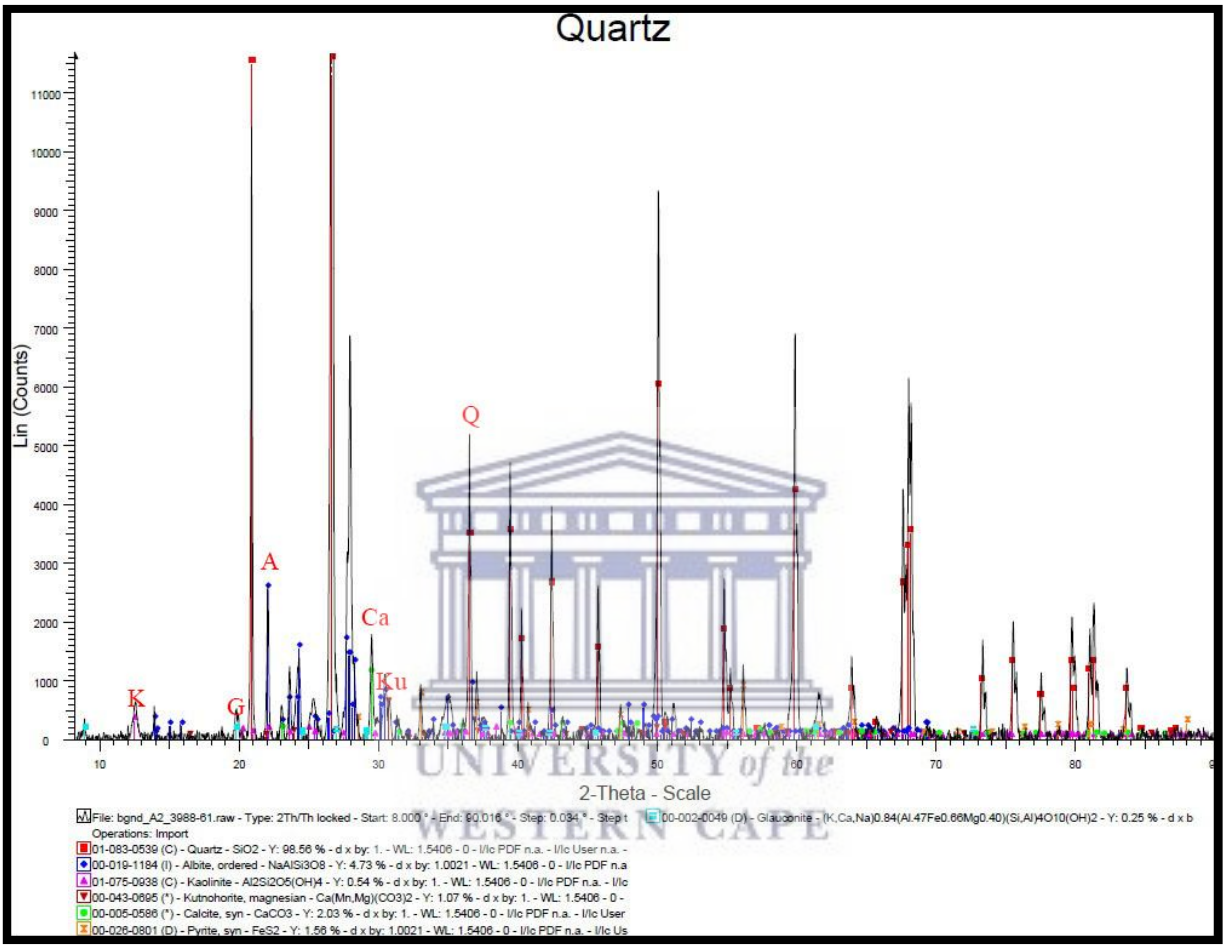

Figure 13: 3988.61m. Q ~ quartz, A~ albite, K ~ kaolinite, Ku ~ kutnohorite, Ca~ calcite, P ~ pyrite, G ~ glauconite

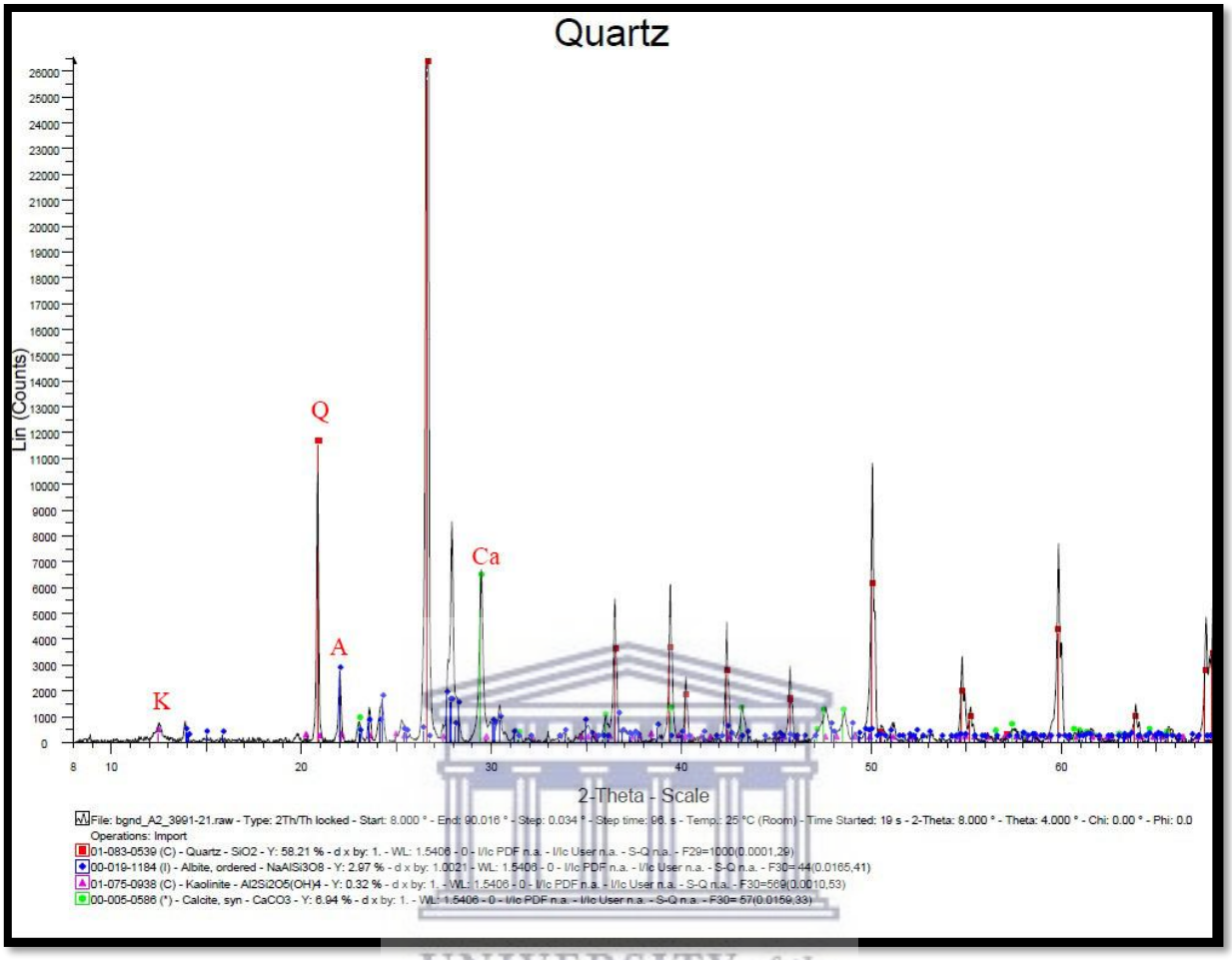

Figure 14: 3991.21m. Q ~ quartz, A ~ albite, K ~ kaolinite, Ca ~ calcite

Well K-A3-Core 1

Figure 15 shows quartz as the most dominant mineral followed by albite. It is observed in all wells that quartz cement are quite pervasive and may have served as a detrimental factor to reservoir quality. The sources of silica remain unresolved, however, there are investigations that have suggested that enormous amount of water, released through compaction could have released silica and therefore precipitated as quartz (Baccar & Fritz, 1994). Furthermore, Morad *et al*., (1990) proposed several other possible sources of silica: detrital feldspar-related sources, pressure dissolution and stylolites within sandstones, dissolution of amorphous silica of biogenic origin or an external source.

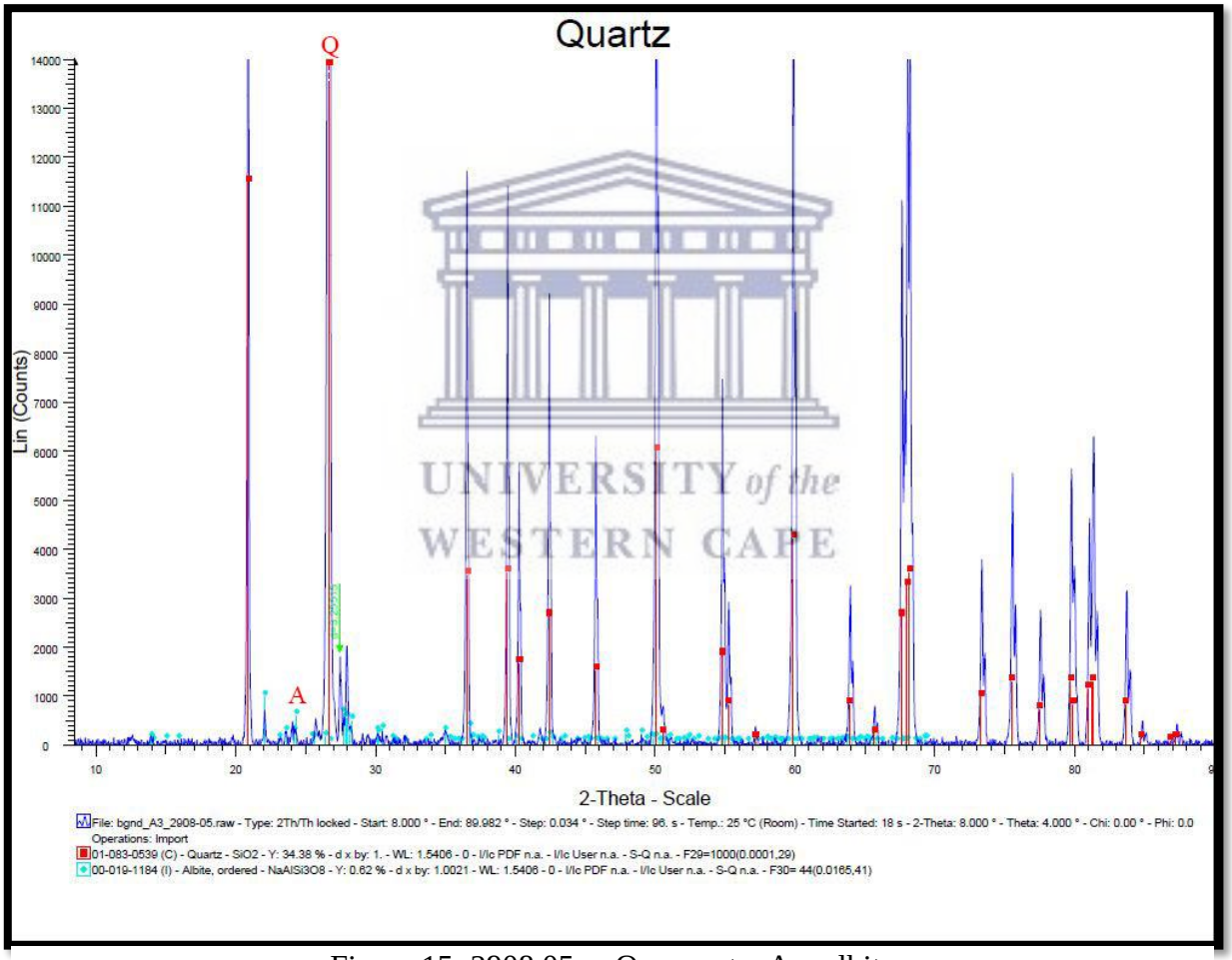

Figure 15: 2908.05m. Q ~ quartz, A ~ albite

Well K-A3-Core 2

As mentioned earlier, the presence of kutnohorite was associated with Mn-rich deposits. Pyrite is common in shallow marine environments; the sulphide was most likely sourced from reduced marine aqueous sulphate (Bukar, 2013) and furthermore signified that sandstone bodies within core 2 of well K-A3 were deposited in an anoxic environment. The presence of calcite at depth 3876.57 m and absence of calcite at depth 3880.10 m, suggested the dissolution of detrital carbonate rock which then may have been flushed by meteoric waters to particular reservoirs within well K-A3.

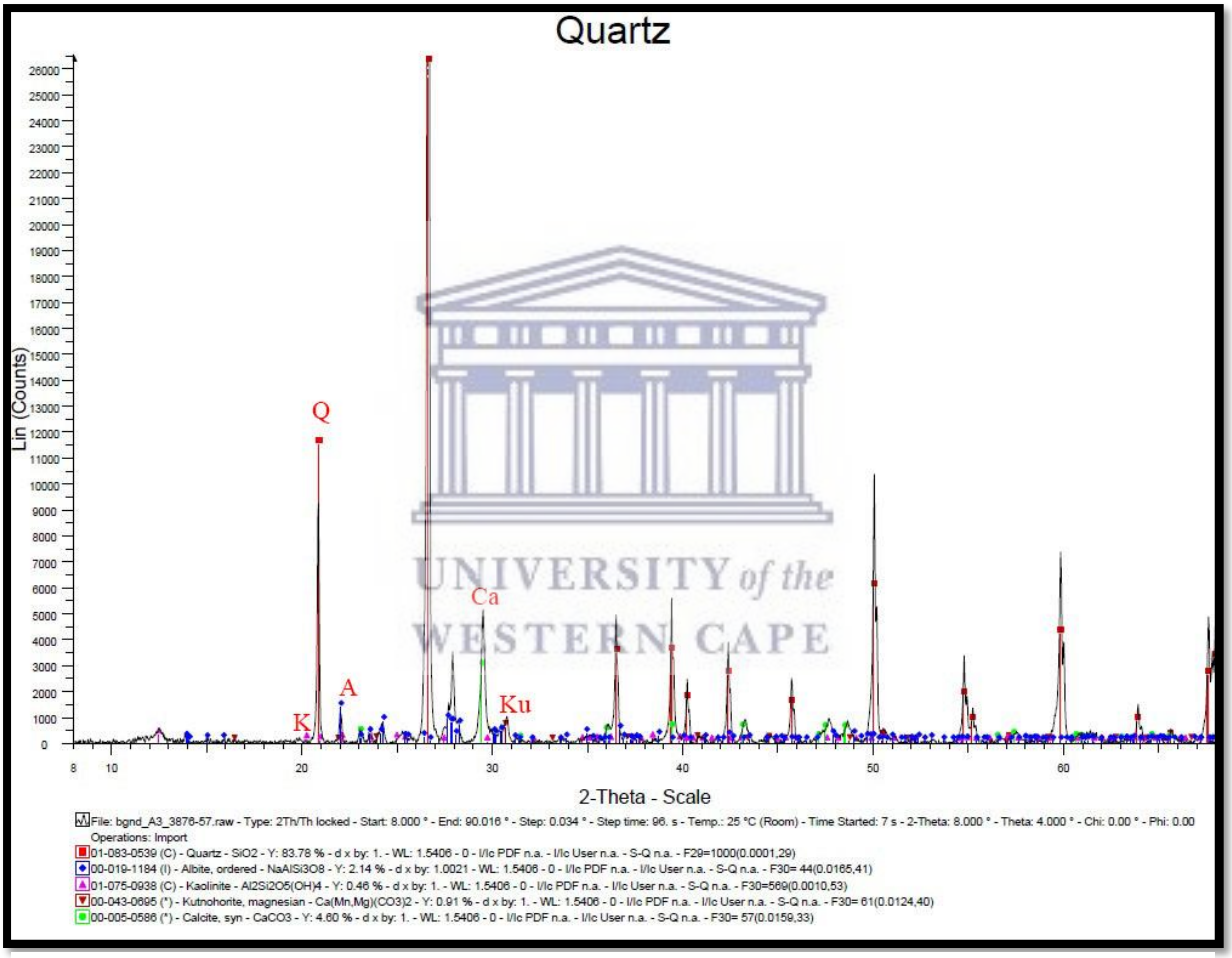

Figure 16: 3876.57m. Q ~ quartz, A ~ albite, K ~ kaolinite, Ku ~ kutnohorite, Ca ~ calcite

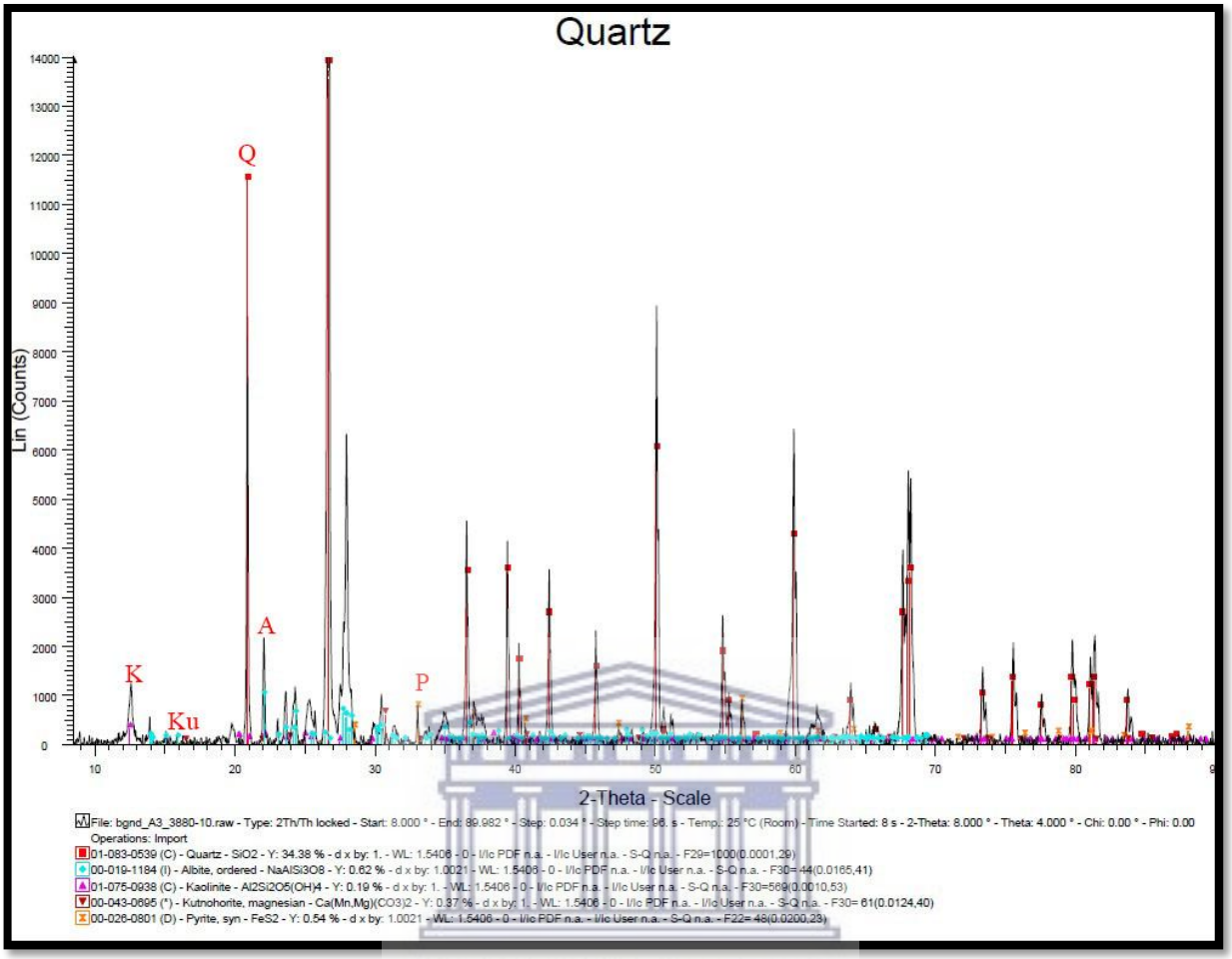

Figure 17: 3880.10m. Q ~ quartz, A ~ albite, K ~ kaolinite, Ku ~ kutnohorite, P ~ pyrite

Well K-E1

The consistent occurrence of kaolinite along with albite in well K-E1 suggested the alteration of feldspar was the predominant process for the formation of kaolinite. The alteration of feldspars occurred by the selective attack on the Al-sites (Naqvi, 2013). The dissolution of feldspar is given in equation 3. The presence of HCO_3^- from meteorite water could have provided hydrogen ions into the pore fluids and therefore favoured the precipitation of kaolinite.

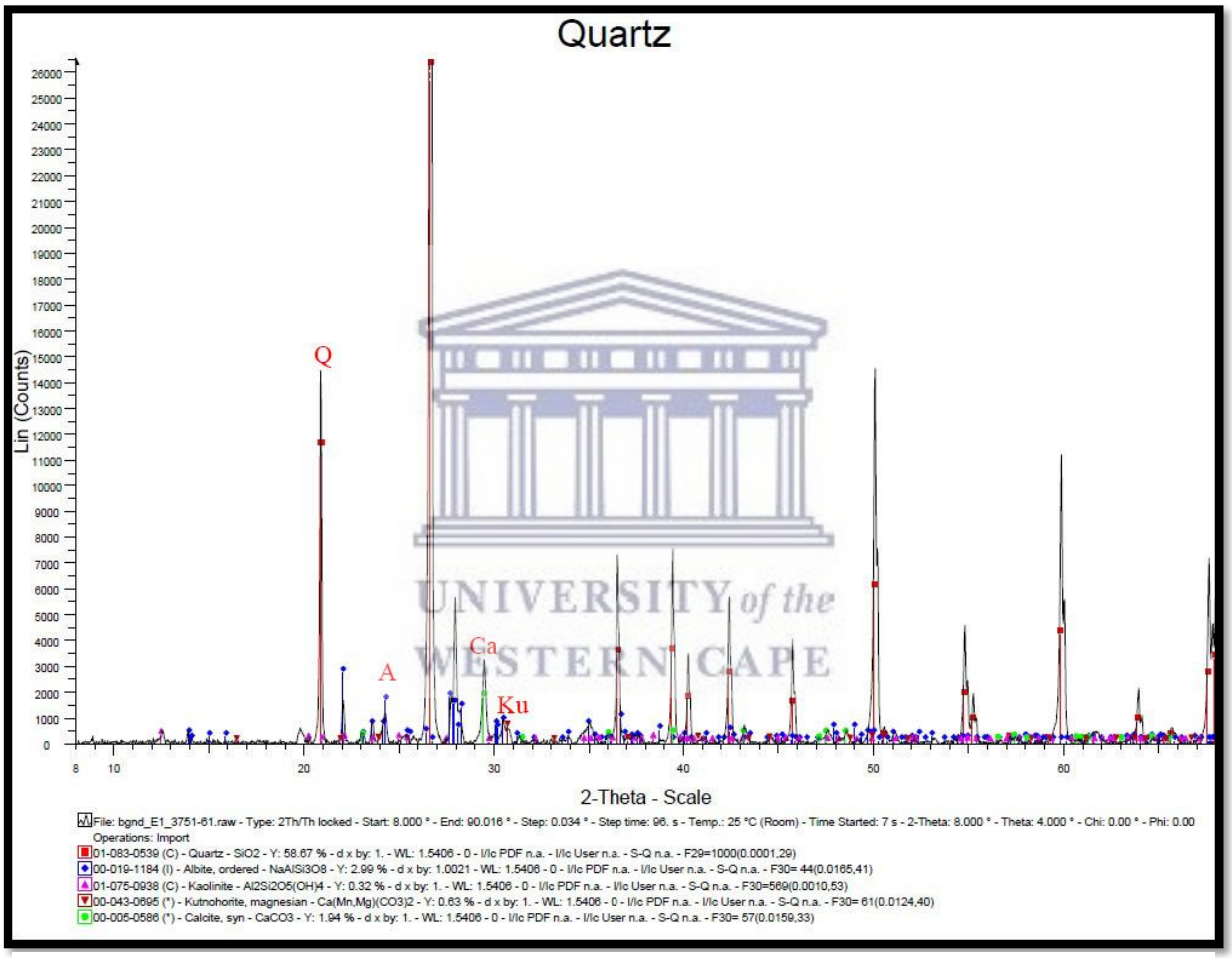

Figure 18: 3751, 61m. Q ~ quartz, A ~ albite, K ~ kaolinite, Ku ~ kutnohorite, Ca ~ calcite

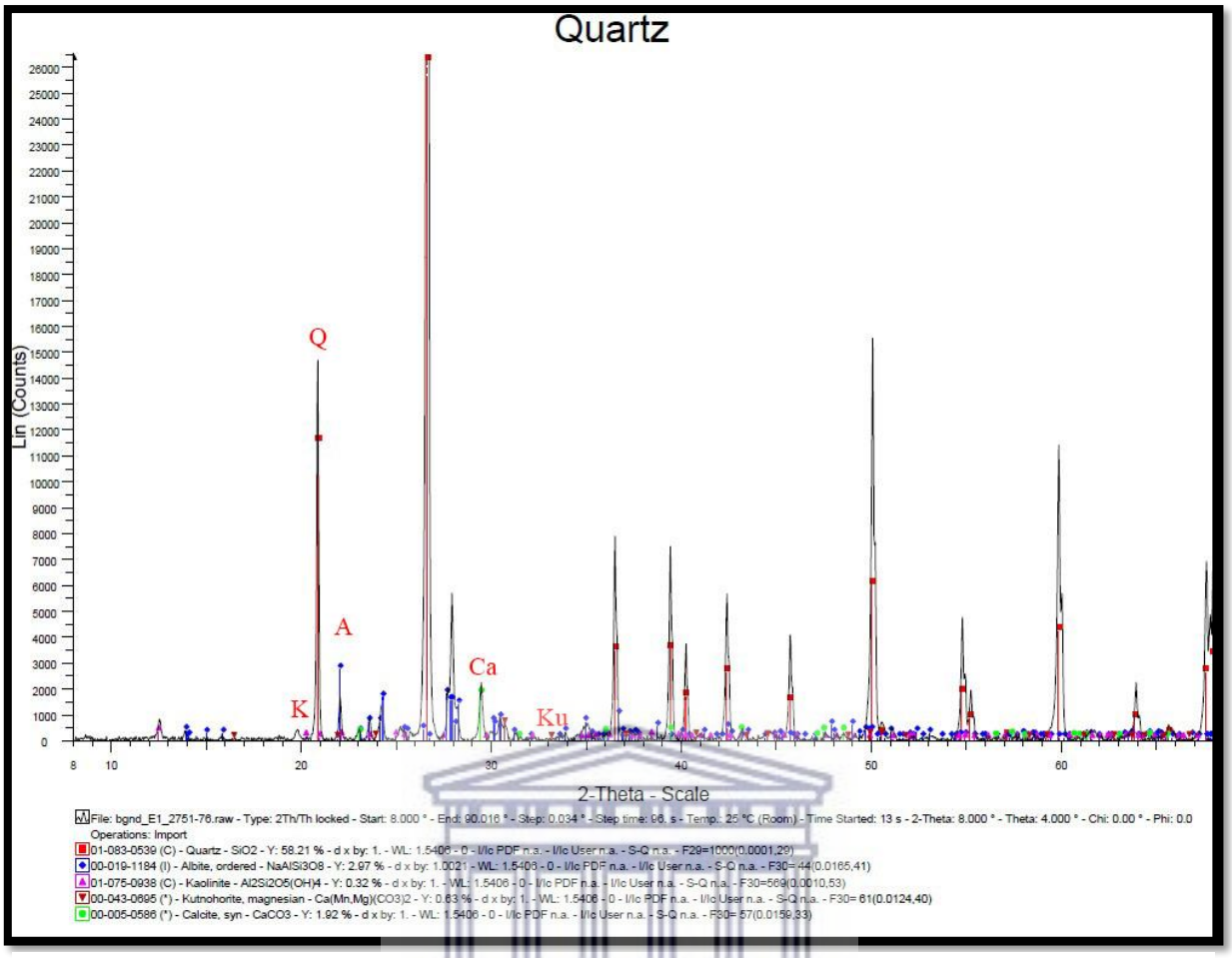

Figure 19: 3751. 76m. Q ~ quartz, A ~ albite, K ~ kaolinite, Ku ~ kutnohorite, Ca ~ calcite

Key insights from the reviewed literature

Quartz cementation was prominent in all three wells along with kaolinite. The occurrences of these two minerals are known to co-exist in shallow marine environments (Hurst & Irwin, 1982). Furthermore, the presence of albite were influenced by the presence of meteoric waters and also served as a precursor mineral for the formation of kaolinite. The source of calcite is envisaged to be bioclasts within well K-A2, whereas in well K-A3 and K-E1, it is thought to be from dissolution of detrital carbonate rock. Moreover calcite cementation confirmed a shallow marine environment. Pyrite within well K-A2 and well K-A3 are indicative of an anoxic environment and could be justified with the core observations (presence of pyrite and its carbonaceous nature). The presence of Iron and manganese in pyrite and kutnohorite respectively are considered to be derived primarily from the breakdown of pre-existing rocks. However, in certain cases sea water can supply a certain amount of manganese and iron to sedimentary rocks (Penrose Jr, 2011).

SEM analysis

SEM analyses were conducted on 8 samples from the wells K-A2, K-A3 and K-E1. SEM assisted in identifying the morphology of minerals, their elemental composition using EDS and also allowed us to look into the pores and analyse the distribution of minerals within and around it.

Well K-A2

Depth 3988.61m

The figures 20 through to 24 shows pore-filling carbonate, kaolinite and albite minerals. The carbonate was identified as kutnohorite which is a member of the dolomite group. Major elements detected by EDX are Ca, Mg, Fe and minor amount of Mn. The relative peaks of the elements corresponded to the chemical formula of kutnohorite. The relatively equal peaks of Na and Al detected by spectrum 91, in figure 23 are due to kaolinite (K) present within the pore. Figure 22 yield the major elements (Na, Si and Al) associated with albite.

From the relics of bioclasts associated with calcite (figure 10), biogenic sources are envisaged to be the primary contributor for the formation of carbonate cements in well K-A2. The kaolin family of aluminosilicates required low ionic strength waters, low pH and are therefore distinctive of weathering profiles and early diagenesis in fluvial and deltaic environments (Worden & Burley, 2009). The deltaic deposits might have allowed the introduction of meteoric waters into the related carbonate units. In addition, the Mg needed for the formation of kutnohorite could have originally been sourced from marine connate waters (Aysee, *et al*., 2010). Moreover, porosity reduction caused by carbonate and kaolinite minerals occurred in the early stage of diagenesis (eogenetic).

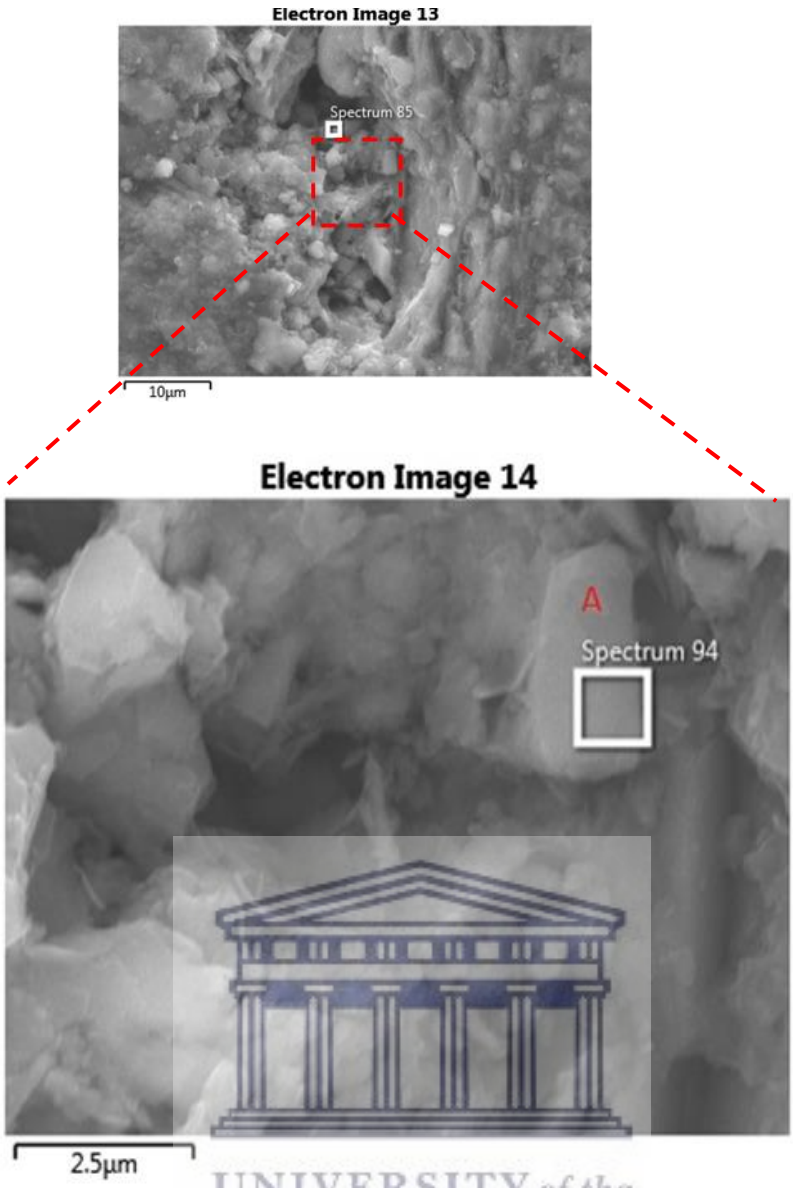

Figure 20: SEM micrograph is an enlargement of the red dashed box and shows well developed albite crystal cemented by kutnohorite. Flaky kaolinites are also present.

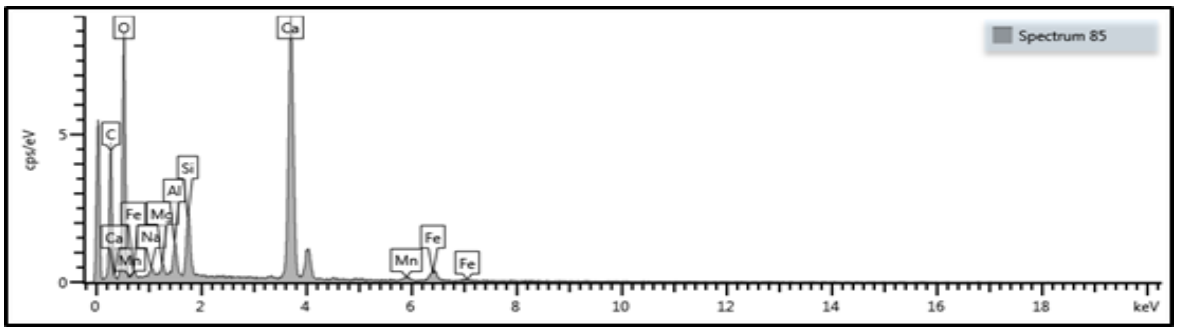

Figure 21: EDS spectrum showing the major elements associated with kutnohorite (Ca, Mg, Fe and Mn). The nearly equal peak heights of Si and Al are associated with kaolinite and the Na.

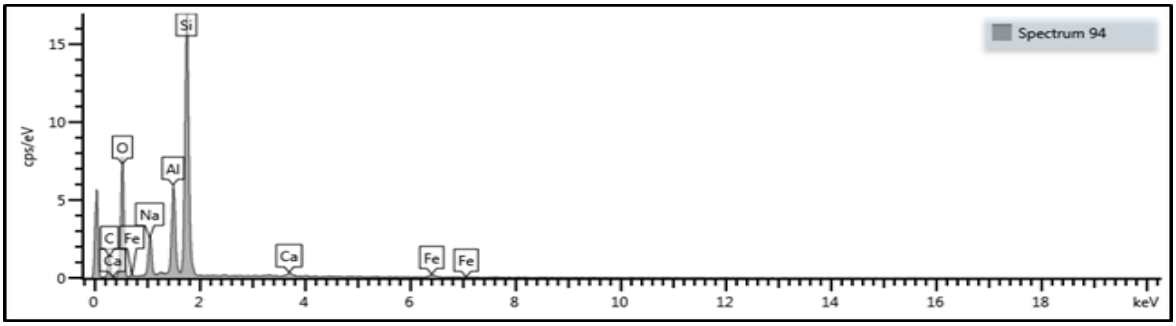

Figure 22: EDS spectrum reveals Si, Na and Al which are the primary elements of albite.

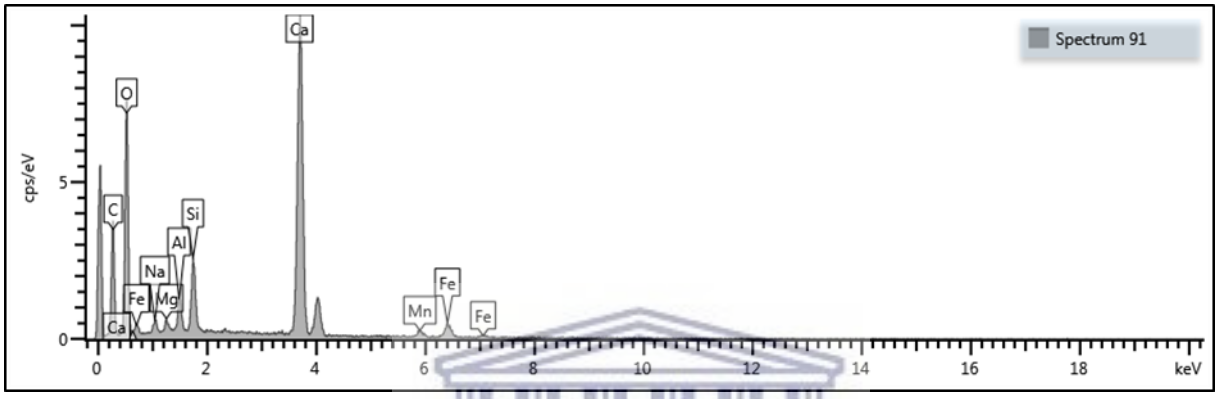

Figure 23: Major element detected by EDS spectrum is Ca with relatively small peaks of Mg, Fe and Mn are distinctive of kutnohorite. The nearly equal peaks of Al and Si are characteristic of kaolinite.

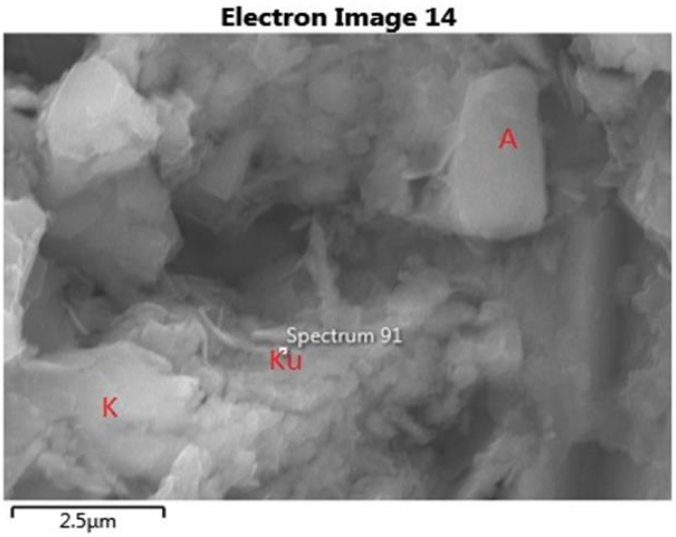

Figure 24: Kaolinite (K) is identified by its flaky morphology along with well-developed albite (A) crystals cemented by kutnohorite (K)

Depth 3991.21m

Figure 25 shows pore-filling calcite (C) cemented by quartz (QC) occurring adjacent to well-developed quartz (QO) overgrowths. Identification of the pore filling calcite was based on the EDX spectrum, yielding Ca as the main constituent and the presence of Si is due to the quartz cement. The presence of Mg and Mn could possibly be due to underlying kutnohorite minerals. The detection of nearly equal peaks of Si and Al suggested the presence of kaolinite. Furthermore, the quartz overgrowths are partially coated with calcite grains. It can therefore be acknowledged that calcite precipitation post-dated the formation of quartz overgrowths.

The source of Silica in the quartz cement has various sources of origin. However, according to the presence of albite, the source of silica was presumably from feldspar alteration reactions as shown in equation 1. The percolation of meteoric waters was responsible for the alteration of feldspars, hence the release of Si ions and thus the formation of quartz cement (Worden & Morad, 2009).

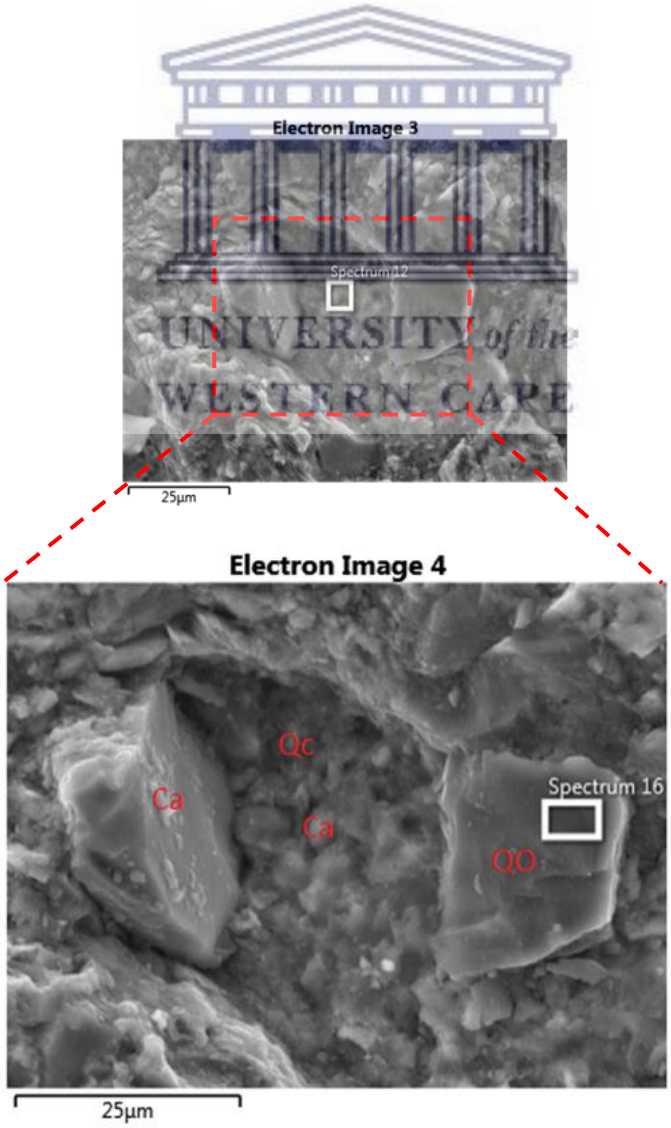

Figure 25: SEM micrograph is an enlargement of the red dashed box. Calcite crystals cemented by quartz cement (QO) are effectively occluding pore spaces. Euhedral quartz overgrowths are to some extent coated with calcite (Ca)

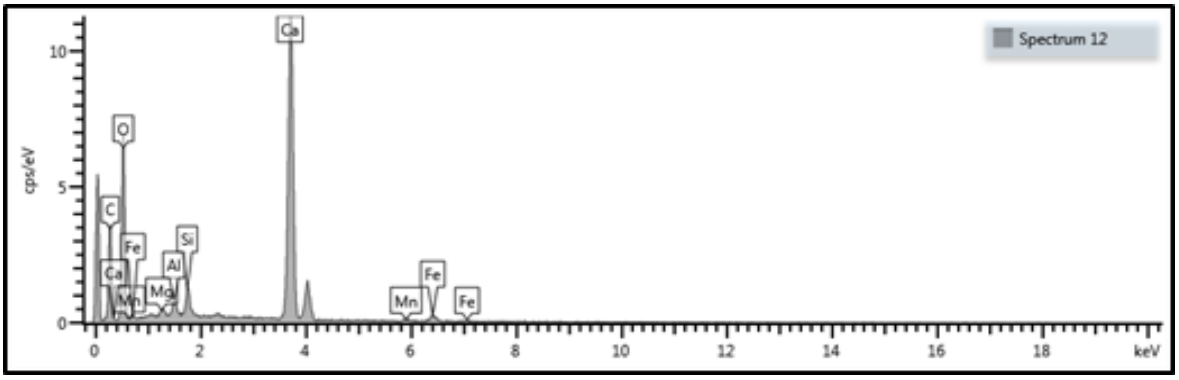

Figure 27: EDS spectrum detected Ca as the major element and is distinctive of calcium. The peaks of Mn, Fe and Mg are too low to consider and is therefore ignored. The nearly equal peaks of Si and Al could possibly be due to surrounding kaolinite.

Well K-A3

Core 1 of well K-A3

Depth 2908.05m

SEM and EDS interpretation

Figure 28 revealed well developed, authigenic albite and quartz crystals that have grown within pore space. A possible source for the formation of albite was the release of Al ions which were liberated from the dissolution of K-feldspar grains (see equation 5). These Al ions re-precipitated at crystallisation nuclei, at favourable diagenetic conditions (Lieu, 2013).

(K-feldspar) $KAlSi_3O_8 + Na^+$ (Albite) $NaAlSi_3O_8 + K^+$ ……equation 5

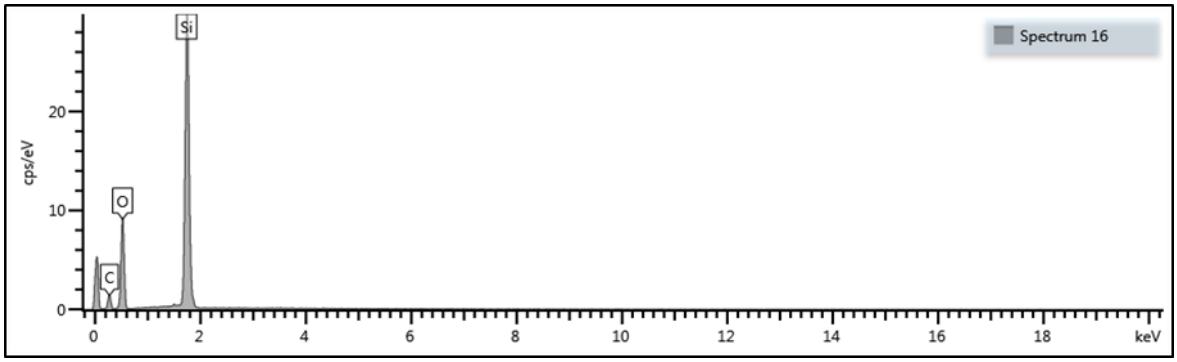

Figure 26: Si is the only major element detected and is characteristic of the quartz overgrowths (QO).

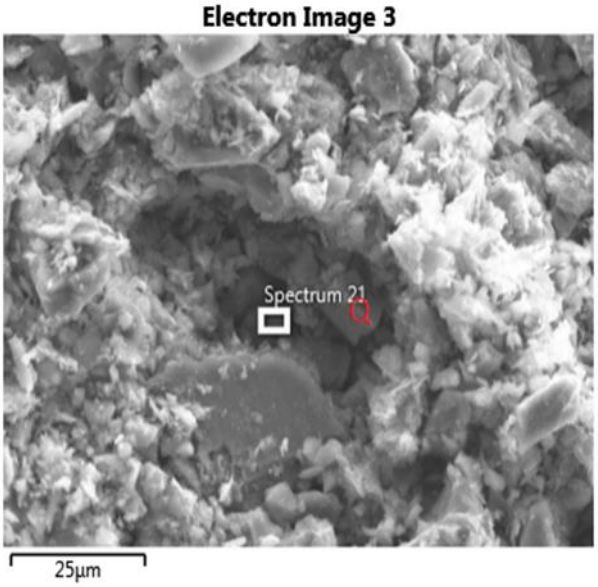

Figure 28: SEM showing pore-filling quartz crystals.

Figure 29: EDS spectrum reveals Si, Na and Al which are the primary elements of albite.

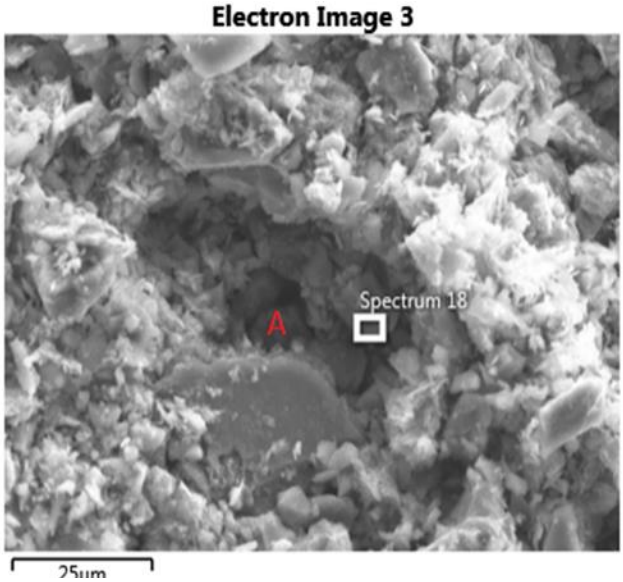

Figure 30: SEM shows pore-filling albite crystals.

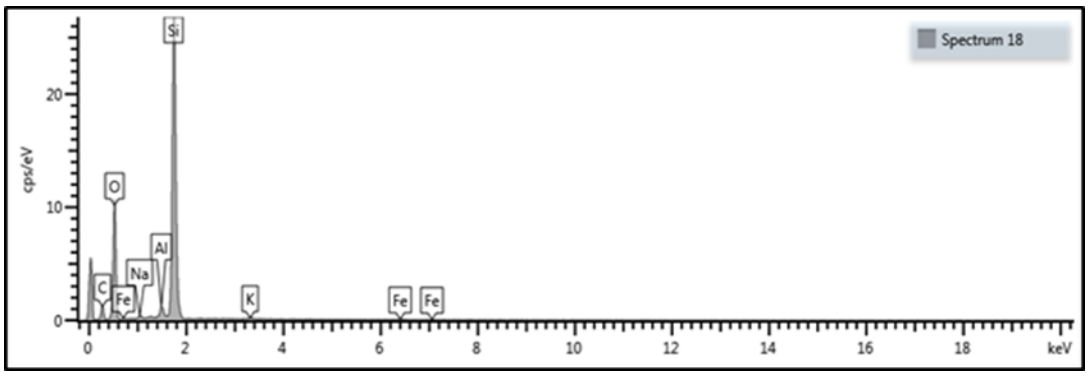

Figure 31: EDS spectrum detected Si as the major element.

Core 2 of Well K-A3

Depth 3876.57m

SEM and EDS interpretation

Quartz overgrowths have been identified in figure 33. These overgrowths are seen to grow within pores. Furthermore, calcite (Ca) and kaolinite (K) occurred as pore filling. Identification of these crystals are based on the EDX spectrum consisting of Si for quartz and nearly equal peak heights of Si and Al for kaolinite. Calcite crystals are seen to have precipitated between the quartz overgrowths.

Figure 33 shows micropores (MP) and microcapillary canals (MC) which may have been important features in transporting dissolved silica from the contact area to surrounding pores (Welton, 2003). Quartz surfaces in figure 38 are completely coated by kutnohorite grains which are furthermore authenticated by spectrum 70 in figure 39 and implying that the sandstone channel experienced influx of connate waters (Mg rich-waters).

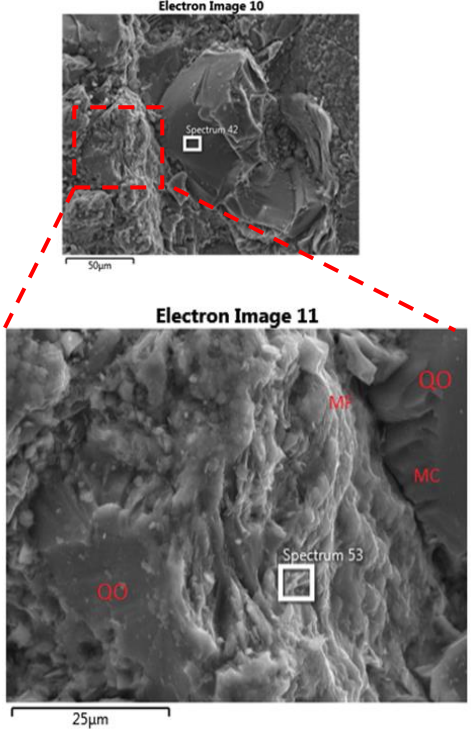

Figure 33: SEM image showing quartz overgrowth creating micro capillary canals and microspores.

Figure 34: Spectrum 42 yields Si as the major element, hence the presence of quartz.

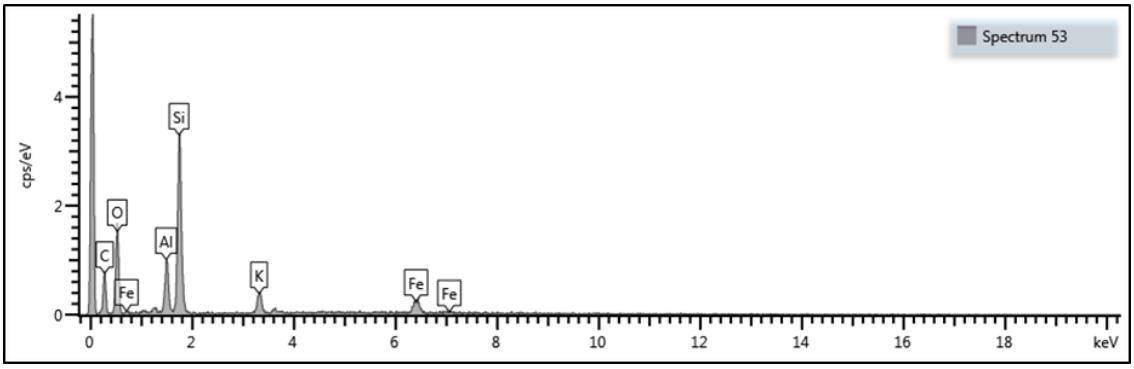

Figure 35: Spectrum 53 yields Si and Al as the major elements of kaolinite.

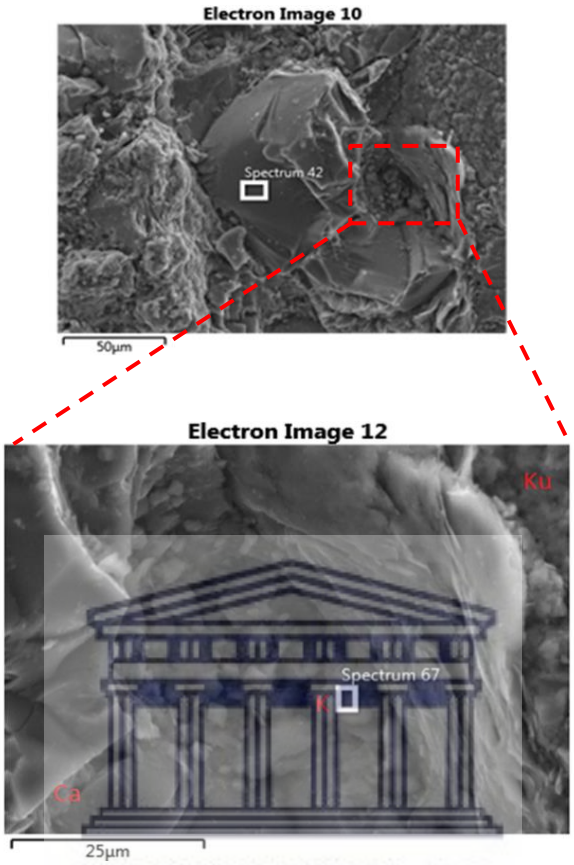

Figure 36: SEM image shows pore-filling kaolinite and calcite.

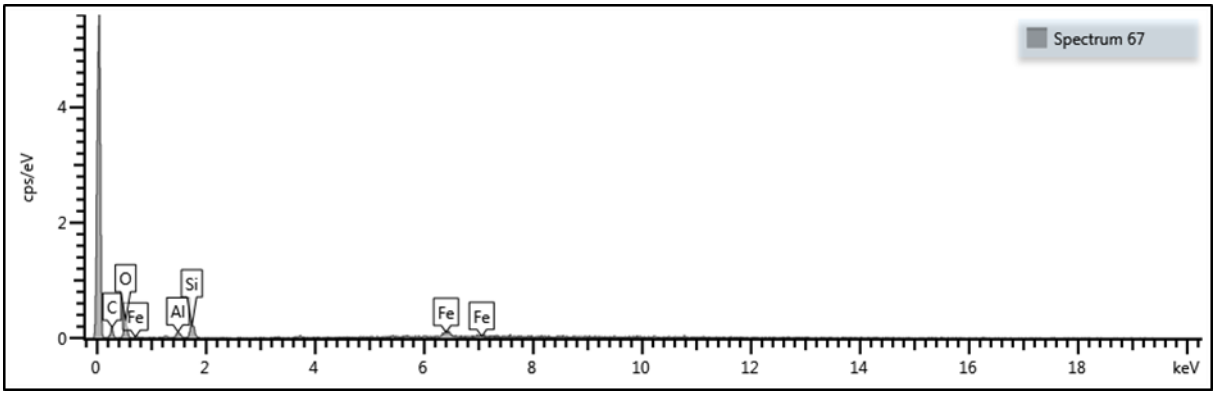

Figure 37: early equal peak heights of Al and Si are associated with kaolinite.

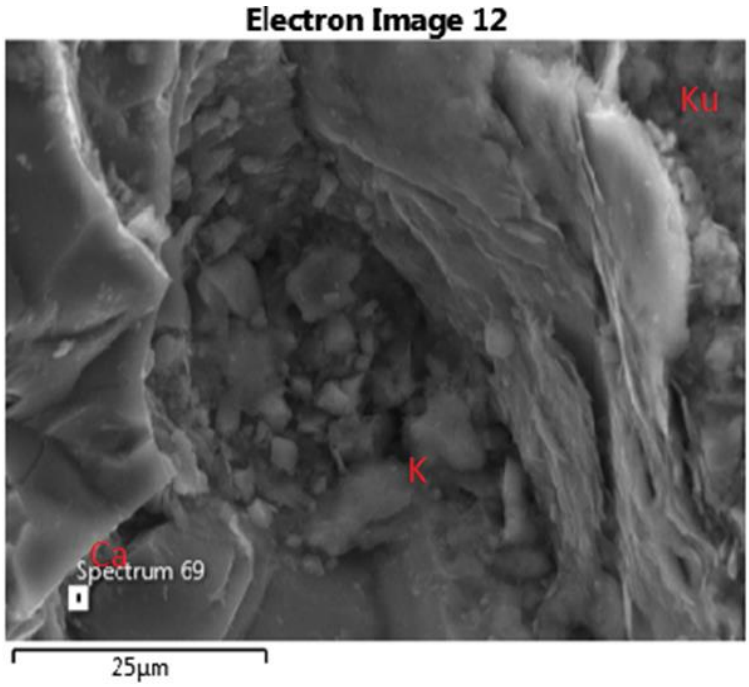

Figure 38: SEM image showing pore-filling kaolinite.

Figure 39: EDS spectrum yields Ca as the major peak, along with low Mg, Mg and Fe peaks. The heights of these peaks are distinctive of kutnohorite.

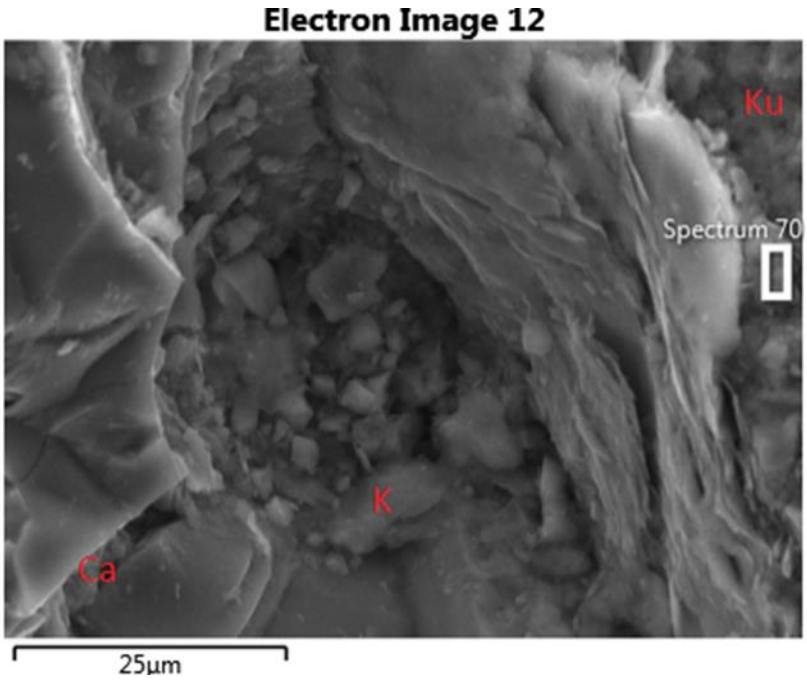

Figure 40: SEM image shows precipitated calcite between quartz grains. Spectrum 70, represented by the white block shows quartz surfaces coated by kutnohorite

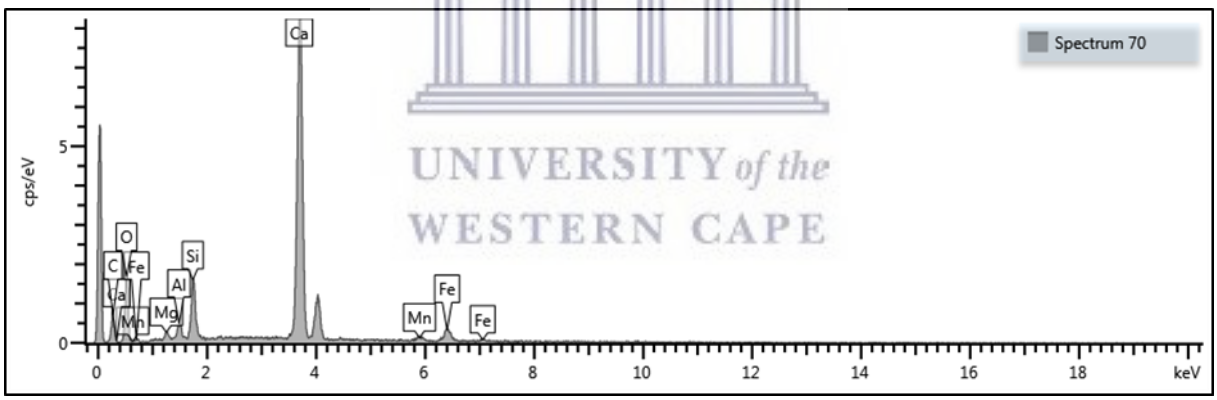

Figure 41: EDS spectrum yielding Ca as the major element along with Al, Fe .

Sample 1 of depth 3880.10m

SEM and EDS interpretation

Figure 42 displays quartz grains that are entirely rimmed by quartz overgrowths (QO) and obscures the grain rounding. The overgrowths are overlain by a subhedral/euhedral cluster of pyrite (Py) crystals. The morphology was distinctive and easily recognisable in SEM. EDS results yield Si and Fe as the major elements. According to Odigi *et al*. 2014. Pyrite can form from partial replacement of organic materials associated with shale laminae. Therefore this

suggested that the pyrite present in core 2 of well K-A3 could have possibly been sourced from the shale laminae observed from the core sample. The presence of pyrite crystals resulted from the microbial reduction of detrital ferric iron and typically the influence of seawater sulphate during early burial (Worden & Burley, 2009), hence revealing a reducing environment. Detection of nearly equal peaks of Al and Si indicated the presence of kaolinite. Furthermore, pyrite and quartz overgrowths occurred as pore-filling, hence reduced the porosity.

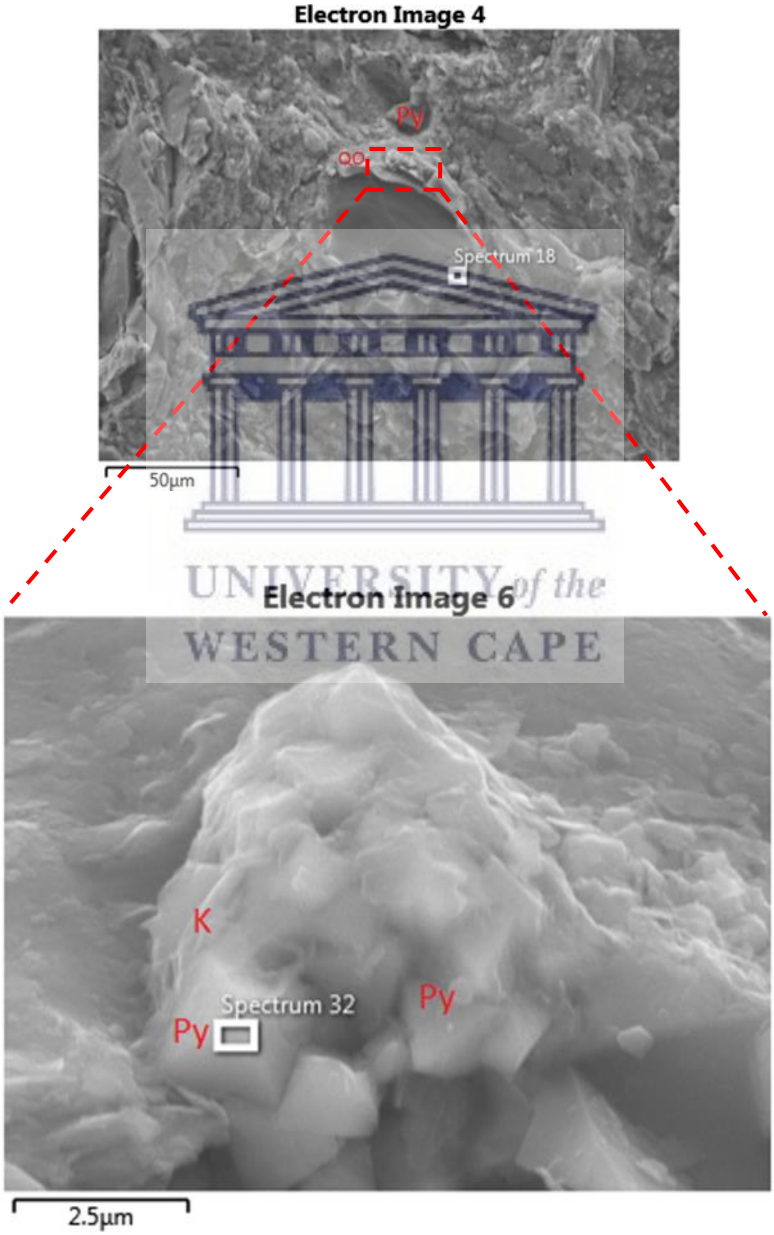

Figure 42: SEM image is an enlargement of the red dashed box. It shows a cluster of subhedral pyrite (Py) crystals overlaying quartz overgrowth.

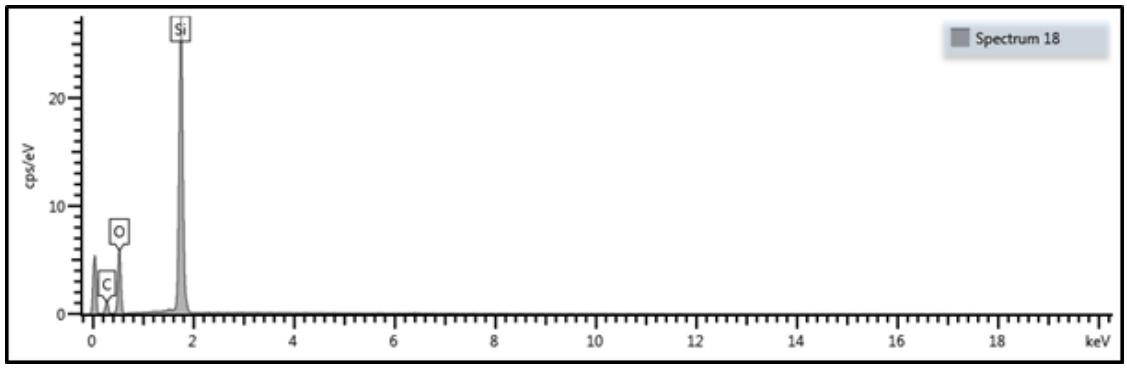

Figure 43: EDS spectrum showing Si as the only major element.

Sample 2 of depth 3880.10m

In Figure 44, kaolinite (K) occurred as discrete particles, mainly in the form of elongate "verms". These kaolinite particles occur as pore-filling between quartz overgrowths (QO). EDS analysis yield nearly equal peaks of Si, Al and XRD results confirm the identification of kaolinite. The arrangement of kaolinite induced microporosity (arrows), aid in the overall reservoir porosity. Authigenic kaolinites are frequently associated with the breakdown of K-feldspars. Such kaolinite crystals essentially had the ability of reducing intergranular pore volume but more importantly served as migrating fines within the pore network (Morris & Shepperd, 1982). The detection of Mg and Fe might have been be due to underlying kutnohorite.

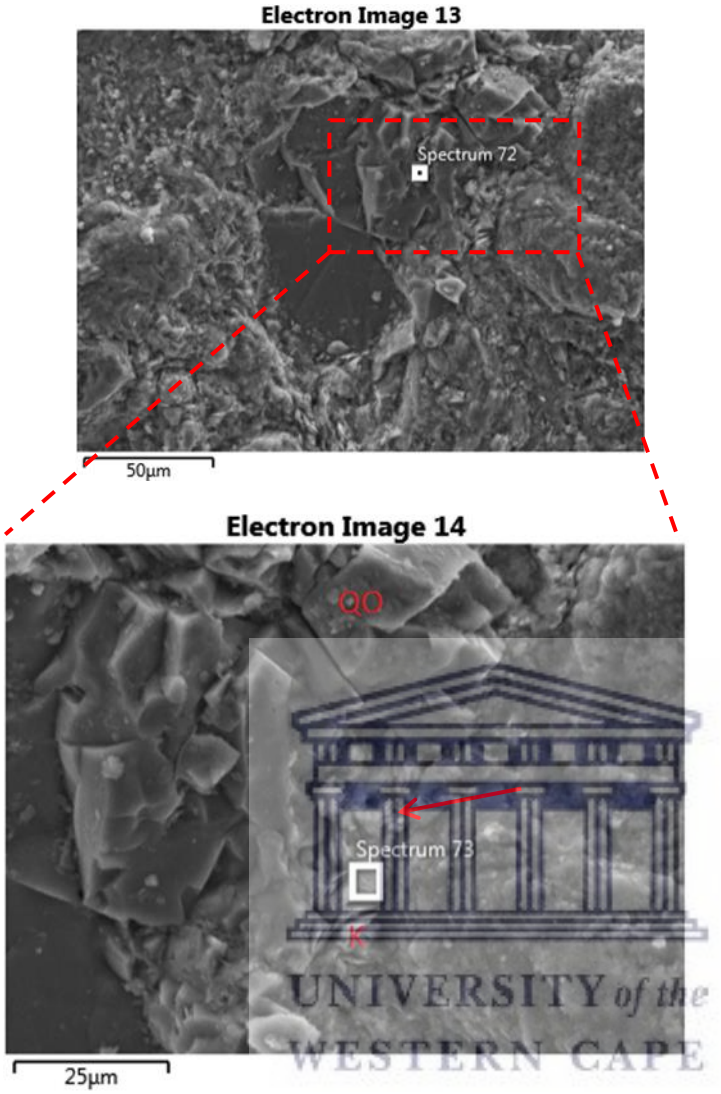

Figure 44: SEM image showing pore-filling quartz overgrowths and "verms" of kaolinite

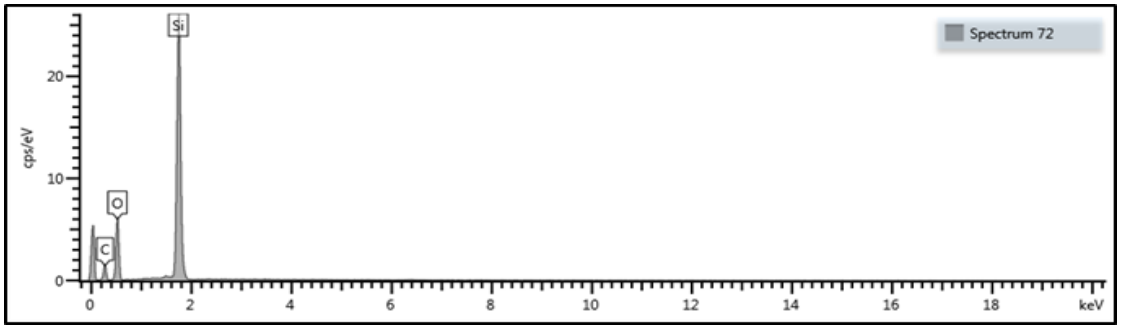

Figure 45: EDS yielding Si as the only element.

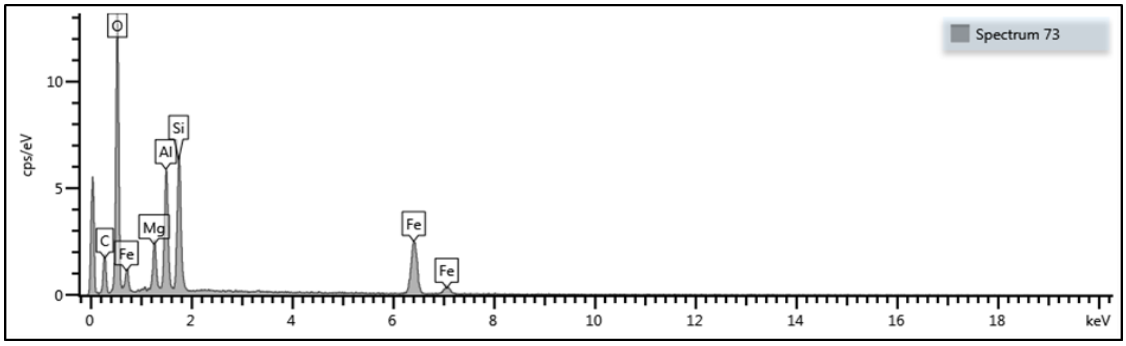

Figure 46: EDS showing nearly equal peaks of Al and SI along with Mg and Fe peaks.

Well K-E1

Depth 3751.61m

Cluster of pore filling kaolinite flakes with relatively minor amount of albite crystals have been identified by the SEM micrograph (figure 45) and EDS spectrum (figure 47). The EDS spectrum yield almost equally peaks of Si and Al, indicative of kaolinite (K). This cluster is rimmed by quartz grains (Q), which in some partsisas partially coated by albite. EDS analysis indicated that the coating consists of Si, Al Na, the relative peak heights are consistent with the formula of albite (A). The formation of albite occurred by two processes, the first of these occurred during increased salinity of formation water. The second process occurred at any point during diagenesis due to the anorthite feldspar end-menber being unstable at all conditions found within sedimentary basins. The second process liberates Al and thus leads to the kaolinite formation.

The precipitation of quartz seemed to be hindered, the reason being that the cluster of kaolinite and the minor amount of albite crystals precipitated within the pore space and thereby occupied growth space. The possible source for quartz authigenesis could be the dissolution of unstable grains (feldspar and ferromagnesium silicates). The arrangement of kaolinite and albite created microporosity/ a tortous micropore system within well K-E1 at the specific depth of 3751.61m.

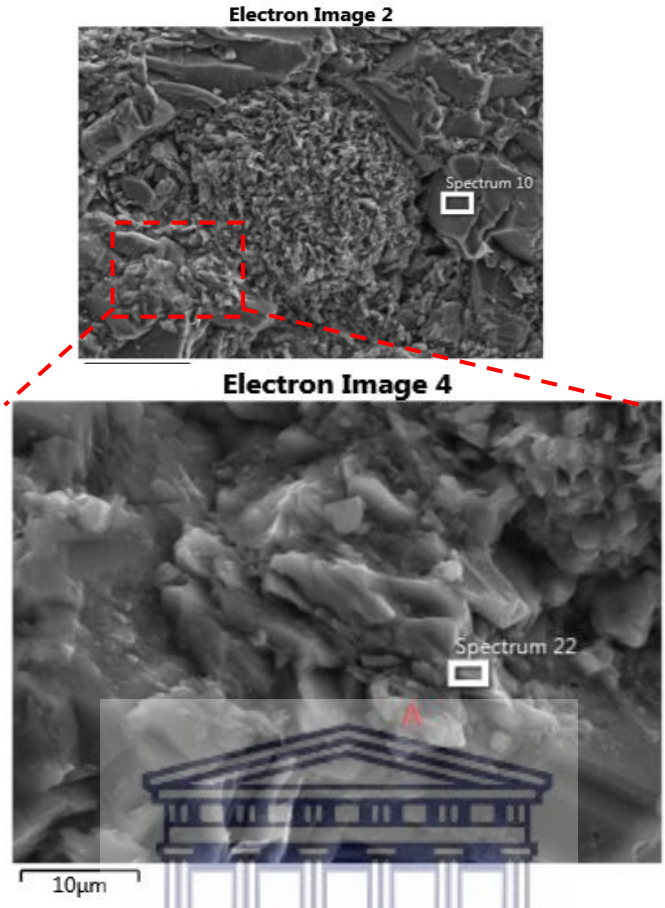

Figure 47: SEM image shows albite crystals grown onto quartz surface.

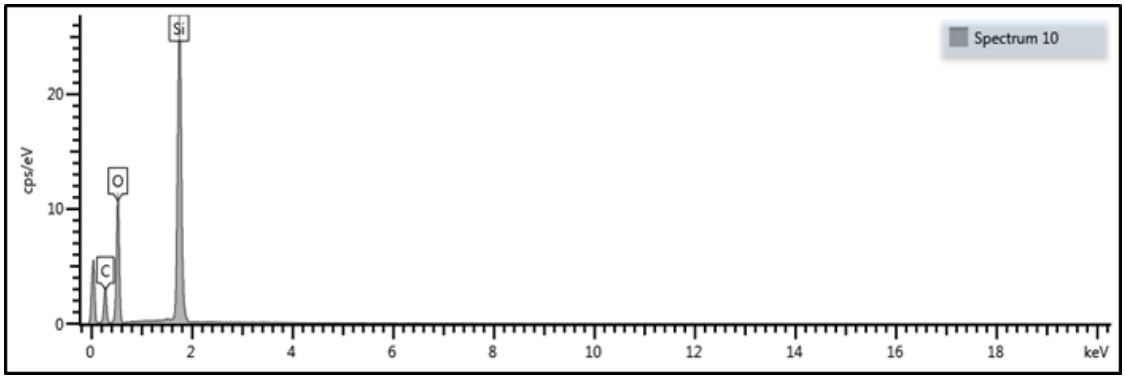

Figure 48: EDS spectrum yields Si as the major element.

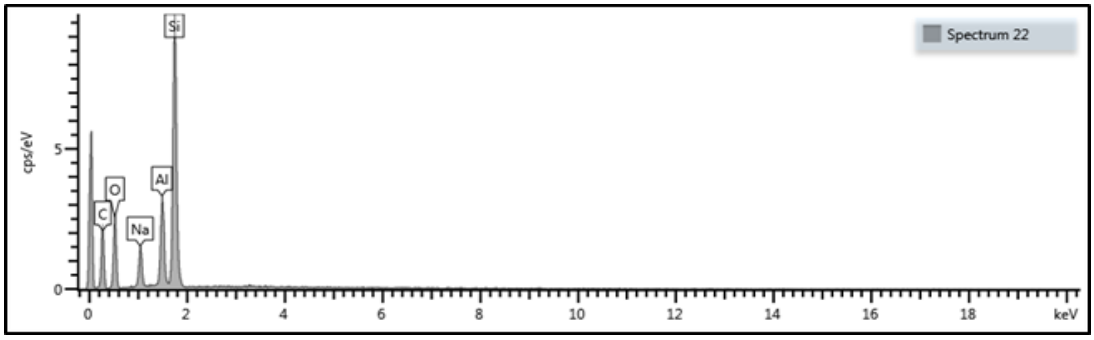

Figure 49: EDS spectrum showing the major constituents of albite.

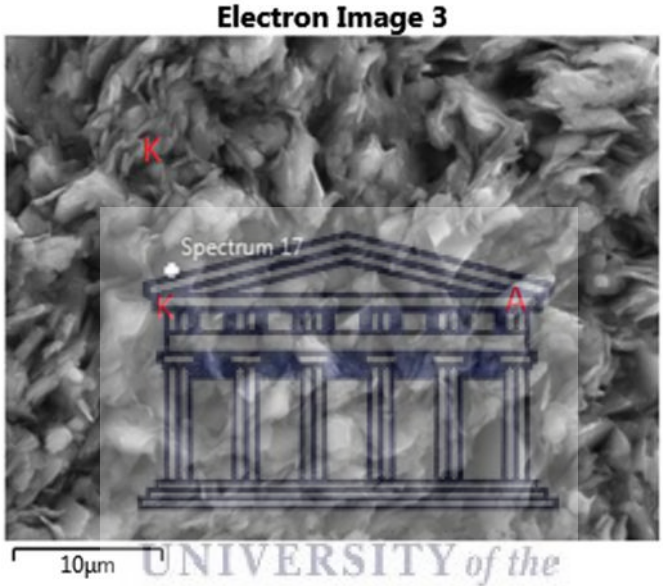

Figure 50: SEM image showing a tortuous micropore network created by the arrangement of pore-filling kaolinite and albite crystals.

Depth 3751.76m

SEM and EDS interpretation

Calcite minerals and quartz overgrowths with nearly perfect crystal habits occludes pore spaces. These overgrowths were partially covered by albite and calcite crystals. This indicated that the quartz overgrowths formed first followed by albite and calcite crystal formation. The quartz overgrowths are possibly associated with meteoric water, which took up SiO_2 liberated from chemical weathering and dissolution processes of unstable minerals such as feldspar. It is evident that quartz overgrowths significantly reduced the size of pore throats and intergranular pores. Accurate identification of the minerals were based on EDS analysis. The albite EDX spectrum revealed the major elements Al, Si, Na and O. The detection of Ca was

most likely due to the presence of calcite. The presence of calcite was further authenticated by the XRD results.

Detrital K-feldspar has a jagged surface (figure 52) with secondary micropores (arrows) and the formation of elongated albite (A) crystals. The albite was identified by EDX analysis and consisted of all the major elements O, Na, Si and Al, whilst the K-feldspar consist of the elements O, Si, Al and K. Albite was precipitated during early diagenesis due to sodium dominated formation water.

Calcite was identified by the EDS spectrum and occurred as patchy pore-filling crystals. The Calcium ions released from albitization according to equation 4 might have precipitated as calcite within the albitization vicinity. The presence of Te (Tellurium) in figure 55 can possibly be attributed to interference.

Figure 51: EDS reveals the primary elements of albite.

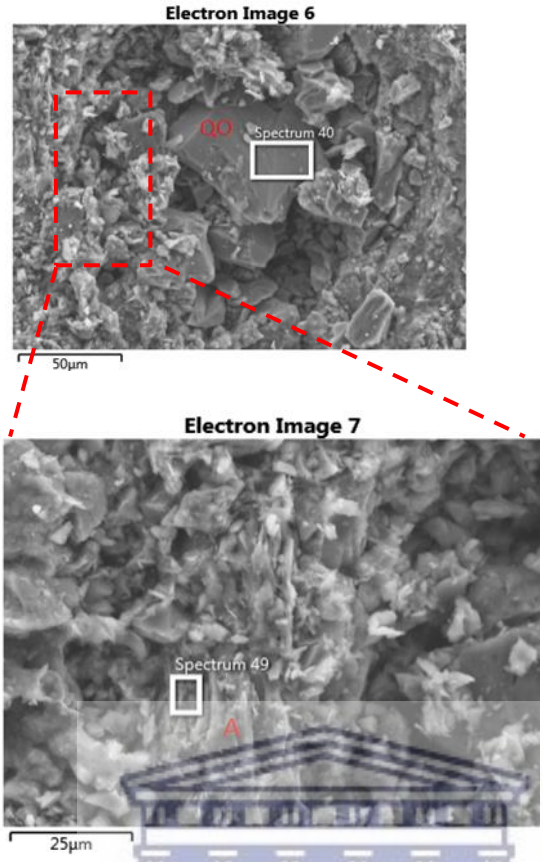

Figure 52: SEM image revealing jagged surface created by albite crystals.

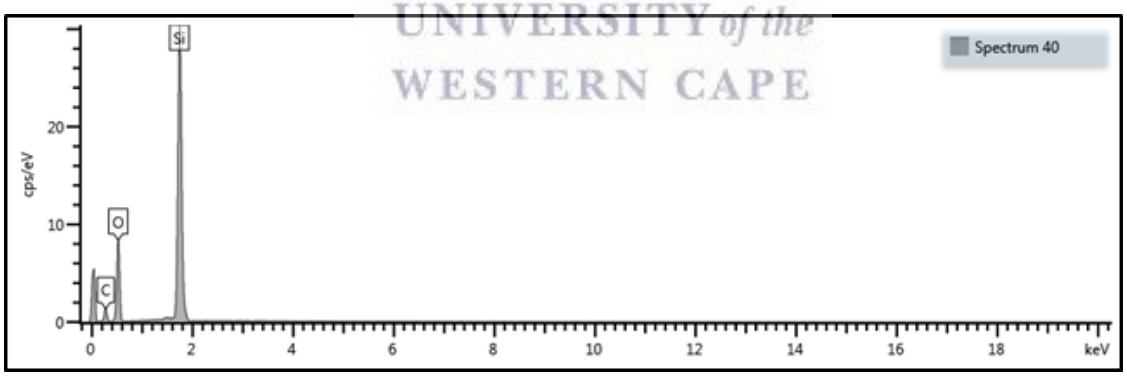

Figure 53: EDS yielding Si as the only element.

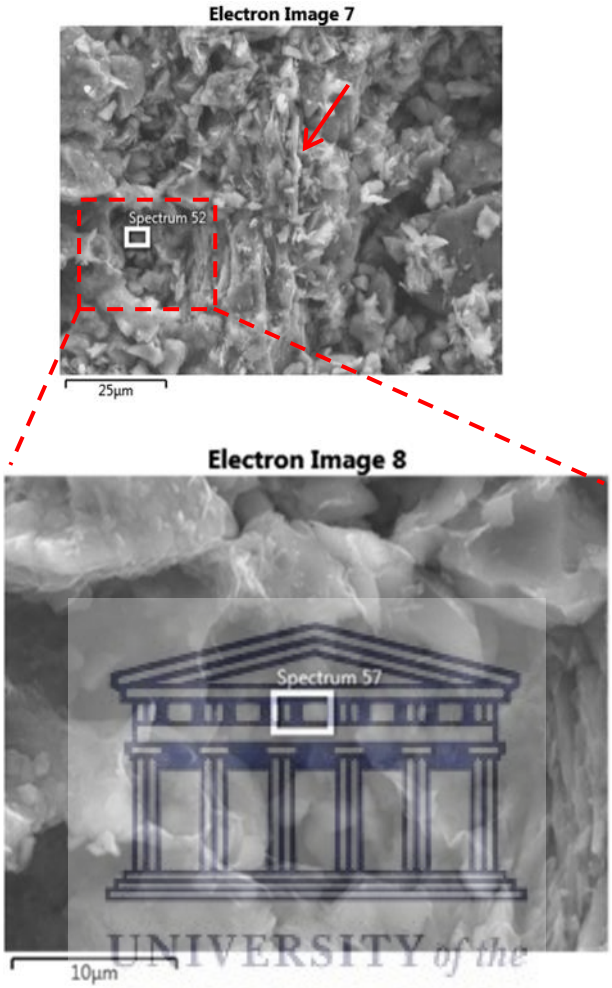

Figure 54: SEM image showing pore space being occluded by calcite cement.

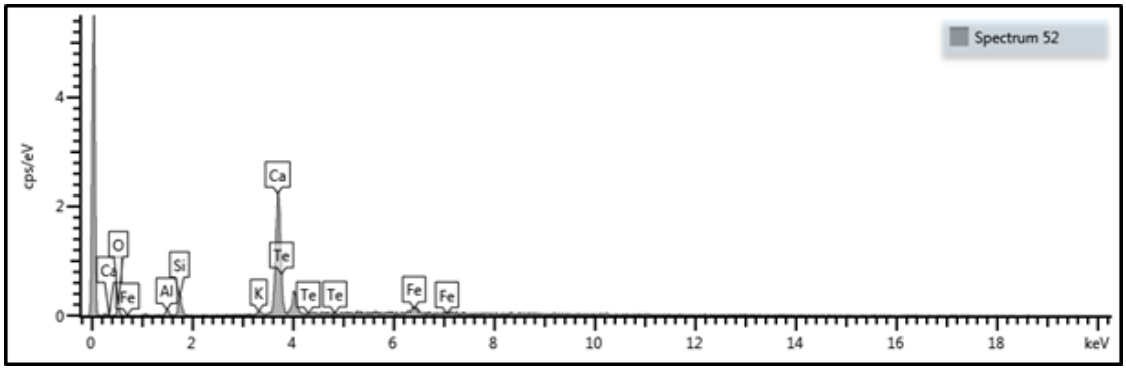

Figure 55: EDS showing constituents of albite and calcite minerals.

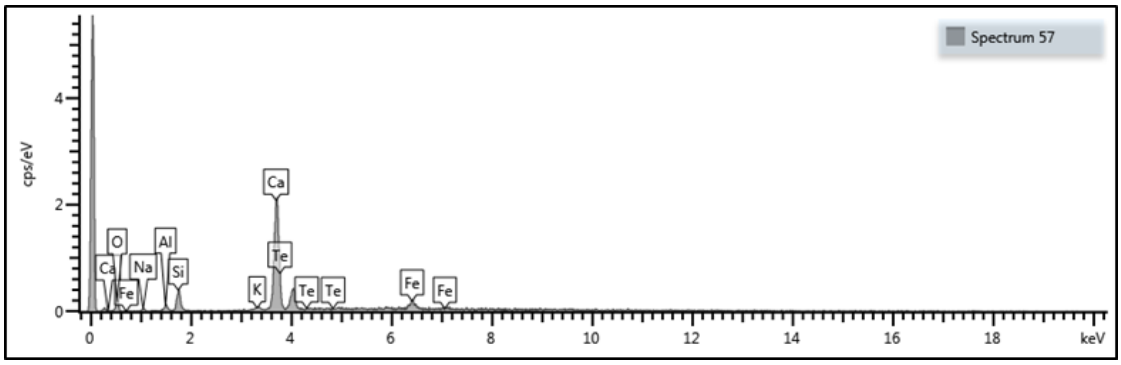

Figure 56: EDS spectrum detected Ca as the major element in conjunction with low Si, Te and Fe peaks.

Key insights from the reviewed literature

Quartz, kaolinite, albite and calcite are recognised as the most dominant reservoir quality destroyers (Kaiser & Richmann, 2008). Well K-A2 consisted mainly of pore-filling carbonate, quartz, kaolinite and albite minerals. EDS spectra show the primary constituents of the above mentioned minerals. Biogenic sources are envisaged to be primary contributor for the formation of carbonate cements. Authigenic albite occluded the pore spaces in well K-A3. A possible source for the formation of albite was the release of Al ions which were liberated from the dissolution of K-feldspar grains. The nearly equal peaks of Al and Si indicate the presence of kaolinite and is identified by SEM as pore-filling. Furthermore, pyrite and quartz overgrowths occur as pore-filling hence reduced the porosity. Kaolinite (K) occurred as discrete particles, mainly in the form of elongate "verms". These kaolinite particles occur as pore-filling between quartz overgrowths (QO). EDS analysis yield nearly equal peaks of Si and Al and XRD results confirmed the identification of kaolinite. The arrangement of kaolinite induced microporosity (arrows), which aide in the overall reservoir porosity. Well K-E1 shows a cluster of pore filling kaolinite flakes with relatively minor amount of albite crystals. Furthermore, calcite occurs as patchy pore-filling crystals.

Thin section analyses

Well K-A2

Well K-A2 reveal sub rounded to sub angular grains of quartz and K-feldspar. The dominant minerals present are quartz, k-feldspar and calcite. Calcite cement between the quartz grains, filling most of the pore spaces, was identified by its high relief and high birefringence and was furthermore authenticated by the XRD results. Well rounded glauconite minerals were identifiable by its green/brown colour which confirms a shallow marine environment (Adams, Guilford, & Mackenzie, 1984) within sample 3988.61 m of well K-A2. Pyrite was observed as single grains, which occluded pore spaces towards the bottom of figure 57 and also as cement in the right side of figure 56. Organic matter along with pyrite is seen on the left in figure 57, organic matter is therefore considered to be the major control for pyrite formation where dissolved iron and sulfate minerals were abundant (Berner, 1984). Furthermore, pyrite occurred as grain coating around the quartz grains and therefore reduced the permeability within sample 3988.61 m of well K-A2 (as seen in figure 57). Calcite filled fractures were identified in figure 59. Moreover, transparent coating was also noticeable in figure 59. The coating was not identified as clay as it is semi translucent; thereby it is inferred to be a shale clast that has been deposited along the top of mineral surfaces.

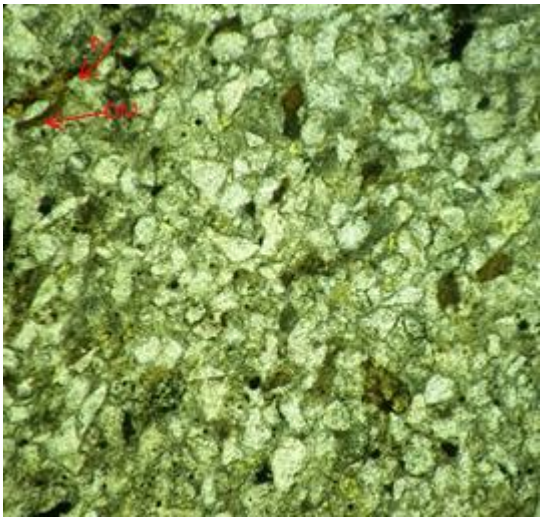

Figure 57: 3988.61m. Plane polarised light (PPL). Organic matter along with pyrite (Py) is seen towards the left in this figure.

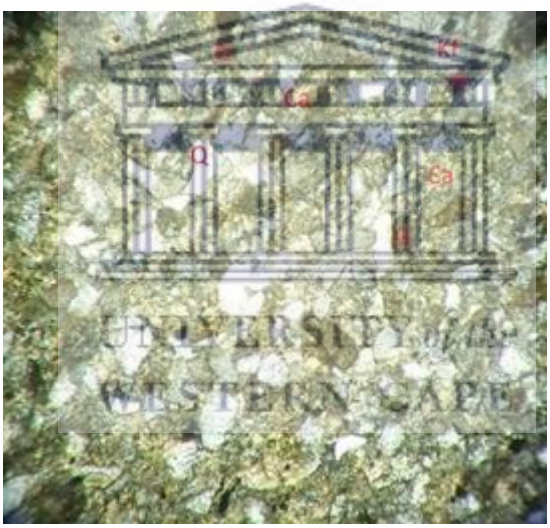

Figure 58: 3988.61m. Cross polarised light (XPL). Calcite (Ca) is filling the pores and reduces the porosity. Quartz (Q), glauconite (G), plagioclase (P), organic matter (OM) and K-feldspar (KF) are seen in this figure.

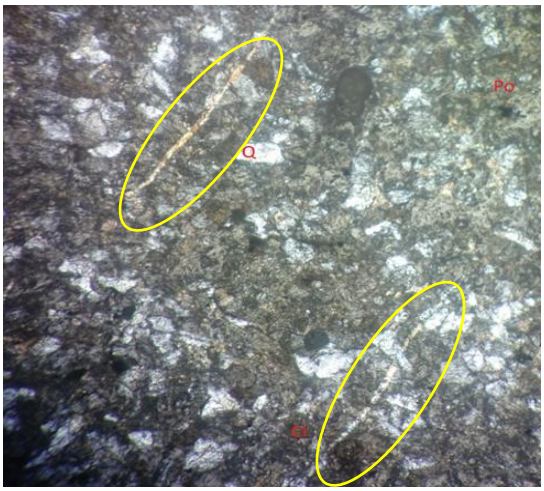

Figure 59: 3991.21m. Calcite filled fractures, along with angular quartz, k-feldspar and calcite/clay cement.

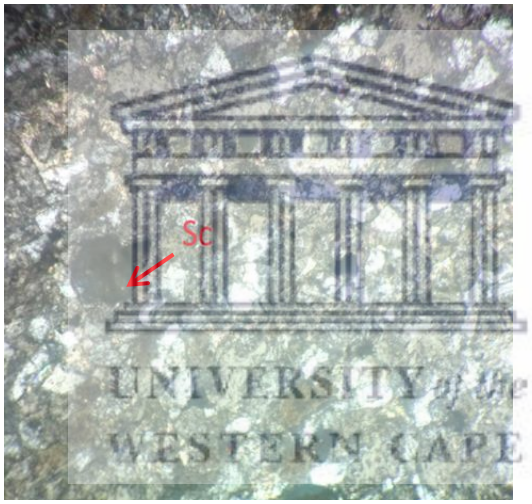

Figure 60: 3991.21m. Shale clasts deposited on the surface of calcite minerals.

Well K-A3

The thin section samples were taken from depths 2908.05 m, 3876.57 m and 3880.10 m. Well K-A2 consisted predominantly of angular quartz and K-feldspar grains. Figure 61 displays coarse grains sandstone, whereas figures 62 and 63 displayed more fine-grain minerals. The petrographic observation in figure 61 shows mechanical compaction of quartz grains. Additionally, the presence of flattened quartz is indicative of overburden pressure/compaction. Porosity is therefore severely affected and is coincident with the petrophysical parameters (figure 8). Albite is recognized by its distinct twinning, however it shows a quartz inclusion

which could have most likely been precipitated by Si that was released during compaction/pressure solution and subsequently re-precipitated within the albite. Staining (S) with carbonaceous material is visible as well as the rimming of detrital clay around grains which could have retard/prevent the formation of quartz overgrowth (Bjorlykke, 2010). Figure 62, shows organic carbon staining. Considering the depth of this sample, the presence of organic carbon staining suggested that the sample is in close proximity to a mature source rock. Kaolinte rimming a quartz grain was observed (arrow). The kaolinite presence can be authenticated by the XRD results and according to (Hurst & Irwin, 1982), kaolinite and quartz can co-exist. Figure 63 highlights a stylolite feature that has been filled with quartz cement. Stylolites formed in response to pressure dissolution and are a function of stress on grain contacts (Javid, 2013). The process of stylolisation resulted in the reduction of porosity and permeability and served as a barrier to vertical fluid flow as quartz has precipitated within it.

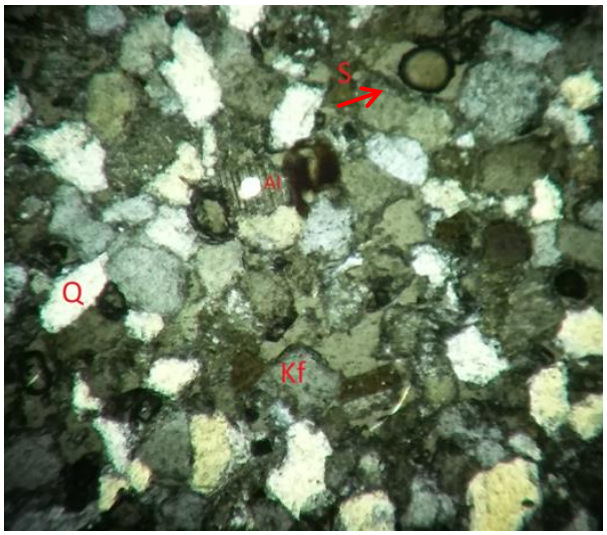

Figure 61: 2908.05m. Coarse grain sandstone, displaying angular shaped quartz and K-feldspar grains. Mechanical compaction of grains along with quartz overgrowths and quartz inclusion within albite are visible.

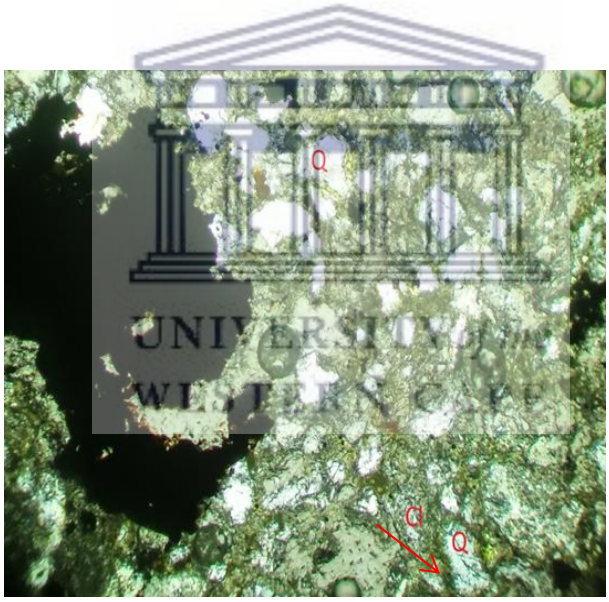

Figure 62: 3876.57m. Organic carbon staining and quartz grain rimmed with clay.

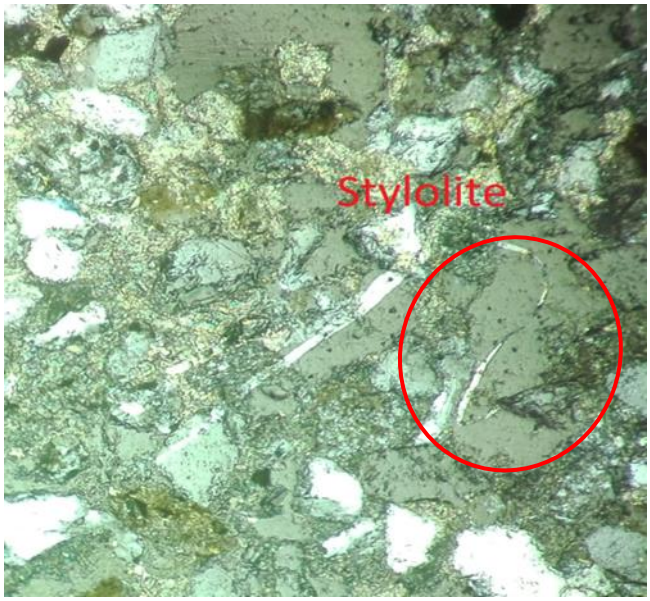

Figure 63: 3880.10m. Quartz filled stylolite.

Well K-E1

Figure 64, displays a strongly consolidated sample with moderately-poorly sorted quartz, kutnohorite (Ku) and K-feldspar grains. The highly birefringent colours (arrow), fine-grained alteration product is most likely sericite (as shown in figure 64). Sericite forms by the alteration of feldspar and it was therefore seen that the sericite does not occur as an isolated mineral. In addition, the sericite is rimmed by clay; this furthermore proves that it is sericite as sericite is frequently intertwined with very-fine grained material and in this case it is kaolinite. The consolidated material is identified as argillaceous material and this was verified by the shaly nature of the core samples. Furthermore, dissolution of feldspar occurred resulting in secondary pore space (Po). It can be inferred that the Fe of kutnohorite (Ku) and Mn were sourced from underlying basement rocks or leached hydrothermally.

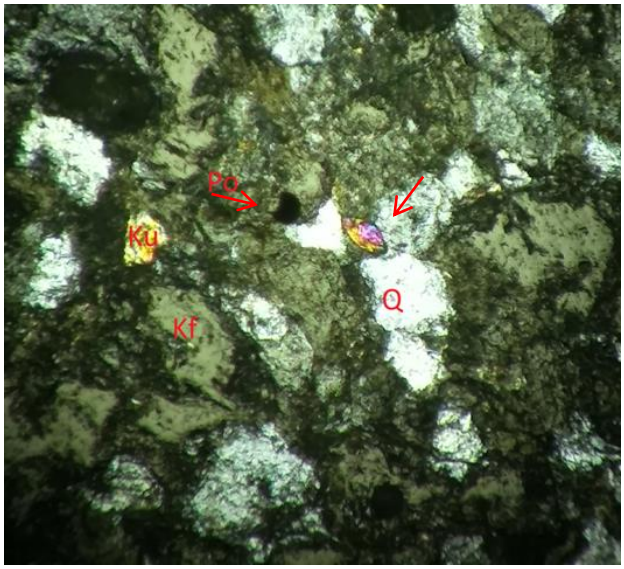

Figure 64: 3751.61m. Moderately-poorly sorted quartz (Q) and K-feldspar grains (Kf) along with random argillaceous material.

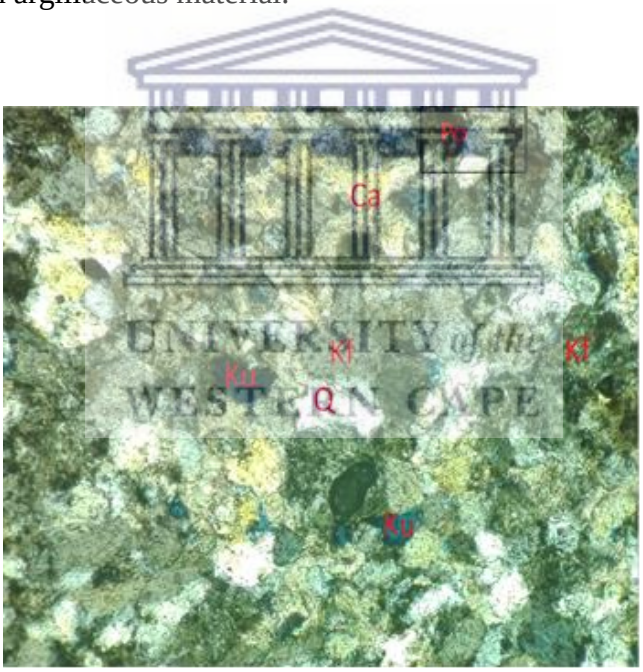

Figure 65: 3751.76m. Calcareous sandstone along with quartz (Q), kutnohorite (Ku) and k-feldspar (Kf).

Key insights from the reviewed literature

Quartz, K-feldspar and calcite are the dominant minerals observed. Well K-A3 shows compaction of minerals, which consequently resulted in elongated quartz (from overburden pressure) and stylolites. The inclusion of quartz within albite formed also in response to mechanical compaction. Quartz grains are rimmed by kaolinite, these two minerals are known to co-exist. Alteration of feldspar in well K-E1 is observed and occurrs along with kaolinite. Calcite cementation is dominant within well K-A2 and K-E1 and therefore serves as a detrimental factor with regards to reservoir properties. The occurrence of glauconite in well K-A2 is indicative of a marine influence and was authenticated by XRD results. Pyrite occurs as grain coating in well K-A2 which was also verified by XRD results. Furthermore, the fracture fillings shown in figure 59, significantly destroys fracture system permeability. Conditions favoring the calcite precipitation might be causally linked to fracture growth, though, i.e. pore fluid pressure fluctuations caused by rapid cement precipitation or they may reflect prevalence of rock-dominated chemistry through much of the rocks burial history, including times when conditions were amendable for fracture growth (Lake, Laubach, & Olson, 2004).

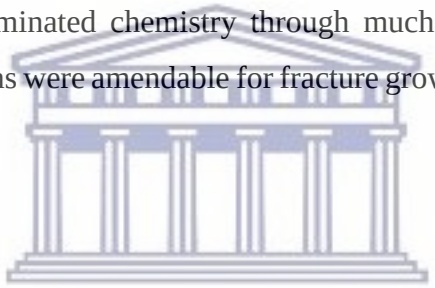

Chapter 5: Conclusion

This study proves that the sandstones of the Lower Cretaceous in the Orange Basin lost porosity and permeability through cementation, clay authigenesis, dissolution and compaction during diagenesis. The presence of calcite and kutnohorite within wells K-A2, K-A3 and K-E1 indicate that they were deposited in a shallow marine environment. The presence of glauconite and pyrite as shown in the thin section of well K-A2 conforms to a marine influenced environment.

Well K-A2 revealed calcite and quartz significantly impeding the porosity (3%) and permeability (0.06mD). Biogenic sources are envisaged to be the primary contributor for the formation of these carbonates cements in well K-A2. Well KA-3 revealed calcite and kaolinite as pore filling minerals which primarily caused the low porosity (10%) within well K-A3 at 3880.1 m. Furthermore, the petrographic observations exhibit mechanical compaction through quartz inclusions within albite mineral grains. Additionally, the presence of flattened quartz is indicative of overburden pressure/compaction. Due to the presence of pore filling kaolinite

flakes with relatively minor amount of albite crystals within well K-E1 (3751.61m) the porosity was reduced (10%) in comparison to the rest of the reservoir interval

The pervasiveness of quartz and kutnohorite cements are considered to be the main reservoir challenges within this study and has proficiently compromised the quality of reservoirs within the Orange Basin. Apart from the above mentioned minerals, pore-filling kaolinite, observed from all analyses has mainly been formed from the alteration of feldspar under adequate conditions, along with calcite are the most prominent porosity and permeability destroyers, thus the low petrophysical values observed were due to the presence of these minerals. Different diagenetic processes such as compaction, cementation, and dissolution of K-feldspar, stylolisation and clay matric infiltration have severely affected the quality of reservoirs.

In order to achieve more reliable results, more wells of the area could be used to further recognize alterations due to diagenetic effects, along with PEF logs, will be a very useful method for determining mineralogy.

References

Adams, A., Guilford, C., & Mackenzie, W. (1984). *Atlas of Sedimentary Rocks under the Microscope*. *Mineralogical Magazine* (First, Vol. 49). London: Longman Group. https://doi.org/10.1180/minmag.1985.049.350.27

Ali, S. A., Clark, W. J., & Dribus, J. R. (2010). Diagenesis and Reservoir Quality, 14–27.

Baccar, M. Ben, & Fritz, B. (1994). Geochemical modeling of diagenetic reactions " a thermodynamic and kinetic approach, 549–550.

Berner, R. A. (1984). Sedimentary pyrite formation: An update. *Geochimica et Cosmochimica Acta*, *48*(4), 605–615. https://doi.org/10.1016/0016-7037(84)90089-9

Bjorlykke, K. (2010). Petroleum Geoscience From Sedimentary Environments to Rock Physics.

Bjørlykke, K. (1998). Clay Mineral Diagenesis in Sedimentary Basins — A Key to the Prediction of Rock Properties. Examples from the North Sea Basin. *Clay Minerals*, *33*(1), 15–34. https://doi.org/10.1180/claymin.1998.033.1.03

Boggs, S. (1987). *Principles of Sedimentology and Stratigraphy*. *Journal of Chemical Information and Modeling* (Fourth, Vol. 53). New Jersey: Merrill. https://doi.org/10.1017/CBO9781107415324.004

Broad, D. ., & Mills, S. . (1993). South Africa offers exploratory potential in variety of basins South Africa offers exploratory potential in variety of basins, 1993.

Bukar, M. (2013). *Does oil emplacement stop diagenesis and quartz cementation in deeply buried sandstone reservoirs*. University of Liverpool.

Dolores, M., & Cruz, R. (1989). Genesis and evolution of the kaolin-group minerals during the diagenesis and the beginning of metamorphism.

Gringas, M., Pemberton, S. ., & Smith, M. (2015). Bioturbation : Rewroking Sediments for

better or worse, 2015.

Hurst, A., & Irwin, H. (1982). Geological modeling of clay diagenesis in sandstones. Clays and Clay Minerals. *Clay Miner*, *17*, 5–22.

Javid, S. (2013). *Petrography and petrophysical well log interpretation for evaluation of sandstone reservoir quality in the Skalle well (Barents Sea)*. Norwegian University of Science and Technology. Retrieved from http://brage.bibsys.no/xmlui/handle/11250/236212

Jiang, S. (2012). Clay Minerals from the Perspective of Oil and Gas Exploratio. *Intech*.

Kaiser, W. ., & Richmann, D. . (2008). Formation of, *1*, 35–44.

Kamgang, T. (2013). Petrophysical Evaluation of Four Wells within Cretaceous Gas-Bearing Sandstone Reservoirs in Blocks 4 and 5 Orange Basin, South Africa, 142.

Lake, L., Laubach, S., & Olson, J. (2004). Advanced Technology for Predicting the Fluid Flow Attributes of Naturally Fractured Reservoirs from Quantitative Geologic Data and Modeling Final Report for the Period Authors : Jon E . Olson , Larry W . Lake and Steve E . Laubach Issued : November 2004 W.

Lieu, K. P. (2013). *and Pore Geometry in Sandstone Reservoir Rocks Gutachter :* Geowissenschaften der Ludwig-Maximilians-Universität München.

Malaza, N., Liu, K., & Zhao, B. (2013). Facies Analysis and Depositional Environments of the Late Palaeozoic Coal-Bearing Madzaringwe Formation in the Tshipise-Pafuri Basin , South Africa, *2013*.

Morad, S., Bergan, M., Knarud, R., & Nystuen, J. P. (1990). Albitization of detrital plagioclase in Triassic reservoir sandstones from the Snorre Field, Norwegian North Sea. *Journal of Sedimentary Research*, *60*(3), 411–425. https://doi.org/10.1306/212F91AB-2B24-11D7-8648000102C1865D

Morris, K. A., & Shepperd, C. M. (1982). the Role of Clay Minerals in Influencing Porosity and Permeability Characteristics in the Bridport Sands of Wytch Farm, Dorset. *Clay Minerals*, *7*, 41–54.

Naqvi, S. (2013). *Weathering of Precambrian basement and formation of sedimentary particles*

in Scania.

Nelson, S. (2014). Joints form as a result of expansion due to cooling or relief of pressure as overlying rocks are removed by erosion. Joints form free space in rock by which other agents of chemical or physical weathering can enter.

Nichols, G. (2009). *Sedimentology and Stratigraphy* (Second). Sussex: Wiley-Blackwell.

Opuwari, M. (2010). Petrophysical Evaluation of the Albian Age Gas Bearing Sandstone, 324.

Oyanyan, R. O., & Oti, M. N. (2015). Sedimentology and Ichnology of Late Oligocene Delta Front Reservoir Sandstone Deposit, Greater Ughelli Depobelt, Niger Delta. *American Journal of Geoscience*, *5*(1), 12–25. https://doi.org/10.3844/ajgsp.2015.12.25

PASA. (2003). Petroleum Agency of South Africa, 2003.

Penrose Jr, R. A. . (2011). The Chemical Relation of Iron and Manganese in Sedimentary Rocks Author (s): R . A . F . Penrose Jr . Published by : The University of Chicago Press Stable URL : http://www.jstor.org/stable/30054302 ., *1*(4), 356–370.

Samakinde, C. (2013). *ASSESSMENT OF THE EFFECTS OF CLAY DIAGENESIS ON SOME*.

Siddiqui, N. A., EL-Ghali, M. A., Rahman, A. H. bin A., Mijinyawa, A., & Ben-Awuah, J. (2013). Depositional Environment of Shallow-Marine Sandstones from Outcrop Gamma-Ray Logs, Belait Formation, Meragang Beach, Brunei Darussalam. *Research Journal of Environmental and Earth Sciences*, *5*(6), 305–324. Retrieved from http://www.doaj.org/doaj?func=openurl&issn=20410484&date=2013&volume=5&issue=6&spage=305&genre=article

Weibel, R., & Keulen, N. (2008). Diagenesis influencing the porosity of Upper Jurassic reservoir sandstones, Danish North Sea. *Geological Society of Denmark and Greenland Bulletin*, *15*(2003), 9–12.

Welton, J. E. (2003). *SEM petrology atlas*. *Methods in Exploration Series No. 4*. https://doi.org/The American Association of Petroleum Geologists

Worden, R. H., & Burley, S. D. (2009). *Sandstone Diagenesis: The Evolution of Sand to Stone*. *Sandstone Diagenesis*. https://doi.org/10.1002/9781444304459.ch

Worden, R. H., & Morad, S. (2009). Quartz Cementation in Oil Field Sandstones: A Review

of the Key Controversies. *Quartz Cementation in Sandstones*, 1–20. https://doi.org/10.1002/9781444304237.ch1

Yamaguchi, N. (2016). South Africa ' s Energy diversification : Part one. Energy global, (June): 2014-2016